Interactive comments on "Aerosol-type classification based on AERONET version 3 inversion products" by Sung-Kyun Shin et al.

Referee comments are noted in black. Our replies are given in blue.

We would like to thank all Referees for their constructive comments. Please find our point-by-point replies below. We have also attached a revised version of the manuscript with all changes marked.

**Anonymous Referee #1**

Review of Paper by Shin, Tesche, Noh and Muller, "Aerosol-type classification based on Aeronet version 3 inversion products"

In this paper, Shin et al. use some of the AERONET inversion products to characterize aerosol types and to "investigate their seasonal and optical properties." They apply their method to four East Asian cities and they end up with 9 different aerosol types that differ from each other in one or another of the various AERONET parameters. Whether or not the attempt is successful, I will leave to the reader to decide. But the paper does shed some interesting light on the problem of identifying aerosol types and I am recommending it be published after some corrections.

We thank the Referee for this positive assessment.

The paper focuses primarily on the aerosol measured at four eastern Asian sites, namely, Beijing, Seoul, Gosan and Osaka. There are few anthropogenic sources near Gosan, so the authors believe it represents the background aerosol of the region. For comparison purposes, they also included in their analysis Aeronet measurements from three presumably polluted sites (GSFC, ISPRA, and Mexico City), from three sites dominated by biomass burning smoke (Alta Floresta, Mongu, and Abracos Hill) and from three sites dominated by mineral dust (Cape Verde, Banizoumbou, and Dakar).

The AERONET properties used in their analysis are the single scattering albedo (SSA), the size distribution (dV/dlnr) (Actually, the identification is based on the fine mode fraction which they denote FMF). These are supplemented with particle linear depolarization ratio (PLDR). They point out that PLDR is a sensitive parameter with respect to particle shape and can be used to determine whether dust particles are present. The PLDR can be obtained from polarization lidar measurements, but also can be calculated from some of the AERONET data products. The authors mention that the derived PLDR used in their aerosol classification procedure is based on the AERONET measurements at 1020 nm wavelength. They state that, "Values of PLDR between 0.30 and 0.35 represent non-spherical particles … while values close to zero indicate the presence of non-spherical particles." (Page 2 line 26) Presumably one or the other of the "non-sphericals" should be "spherical". (On page 4 line 1 we find that PLDR of 0.02 corresponds to "non-dust" and 0.30 corresponds to "Asian dust.").

The Referee is right. We have corrected the typo. PLDR values close to zero refer to spherical particles.

I do not understand why the authors' are calculating PLDR since they seem to be using it primarily to determine the sphericity of the particles. But the AERONET data set has

sphericity as a derived quantity. Why not just use the AERONET value? I would have expected the authors to compare their sphericity evaluation with that of AERONET, or at least comment on why they are not using the AERONET value.

We would like to elaborate on our rationale. Firstly, we didn't calculate PLDRs. This parameter is now included in the AERONET version 3 level 2.0 inversion product. Secondly, sphericity is no longer provided as a parameter in the AERONET version 3 level 2.0 inversion product. And thirdly, PLDR is physically more meaningful than sphericity as it is a parameter that can also be provided from independent measurements, i.e. with aerosol lidar. In particular, we are applying insights from lidar measurements of PLDR to refine AERONET-based aerosol typing. We have added the following statement to Section 2.1 for clarification:

"*AERONET version 3 level 2.0 inversion products include PLDRs and lidar ratios at 440, 670, 870, and 1020 nm. The parameter sphericity, which was provided in the AERONET version 2 inversion product, has been discontinued in version 3. We hence base this study on PLDR. This approach has the additional advantage that PLDR can also be obtained from independent measurements, e.g. with aerosol lidar.*"

The paper reaches the conclusion that the aerosol in East Asia is mainly due to anthropogenic pollution and that dust aerosols are almost always mixed with other types of aerosol particle.

The introduction is well written and sets the stage for the analysis that follows. The authors use the three parameters, fine mode fraction, single scattering albedo and polarization to define the type of aerosol. The aerosol types that they find are: Pure dust, Dust Dominated Mixtures, Pollution Dominated Mixtures, Non-absorbing Pollution, Weakly absorbing Pollution, Moderately absorbing Pollution, Strongly absorbing Pollution, Biomass-burning Smoke

(It almost seems that a new aerosol type is defined for each variation in the three parameters.)

One of my main problems with the paper is the plethora of acronyms that make the paper difficult to read. For example, we read on page 8 lines 1-3, "The occurrence rate of pure and polluted dust (PD, DDM and PDM) over East Asia is slightly lower (34% -49%) than that of dust-free pollution. PDM is the most frequently detected aerosol type of all types that include dust, i.e., PD, DDM and PDM. The occurrence rates of PDM were…" Some acronyms are introduced and never used again. Thus on page 8 line 21 we read, "…secondary organic aerosols (SOA, Sano et al, 2016). The aged SOA …" The acronym SOA is not found anywhere else in the paper. The paper would be much easier to read and understand if some of the acronyms were spelled out. There is nothing wrong with using acronyms, but when they are piled one upon another, the reader begins to flounder. If the authors insist on using so many acronyms, perhaps they could supply the reader with a look-up table of acronyms.

We understand the Referee's concern that our use of acronyms might get in the way of enabling a pleasant reading experience. We have tried to reduce the use of acronyms as much as possible. We are no longer using acronyms for secondary organic aerosols (SOA), Absorption Angstrom exponent (AAE), Angstrom exponent (AE), brown carbon (BrC), organic carbon (OC), coarse-mode to the total volume concentration (CMFvc), absorption aerosol optical depth (AAOD).

Section 3 presents their results. Figure 4 shows the values of PLDR vs fine mode fraction. The figure is broken up into 7 regions. It would be very helpful in understanding this figure if

the caption would indicate the type of aerosol each region indicates. This information is given in the body of the text in lines 25-27 of page 6, but should be in the caption as well. This is done for Figure 5 and should be done here.

A corresponding statement has been added to the figure caption.

The caption of Figure 4 states that, "The color coding indicates the number of observation data in log scale." The color scale goes from 1 to 900. I suppose this means the number of observations range from 1 to 900. It would seem that most of the "pixels" represent less than about 30 readings with many being less than 3.

It means that the highest found number of cases on a PLDR-FMF bin is 900 (red in the plot). The Referee is correct that many "pixels" contain very few cases. This is also reflected in the number of observations N in Table 2.

Figure 5 shows the size distributions (dV/dlnr vs r) for the seven regions presented in Figure 4. The color scheme makes it hard to figure out what line corresponds to which kind of aerosol. Why not use green and yellow rather than three shades of red?

We have revised Figure 5 for better contrast. We now only use a single y-scale. We have also changed the plot to black and gray lines as well as open and solid symbols to enable a better access to the figure also for colour blind readers.

The second panel of Figure 5 gives SSA vs wavelength. The text (page 6 line 31) states that SSA in Sector B is 0.88. This agrees with the value given in Table 2, but it does not agree with Figure 5 which shows the lowest value of SSA to be about 0.92.

We are sorry for this mistake. It turned out that the SSA values in Table 2 were not correct. We are now giving the correct numbers in Table 2 and in the mentioned part of the text. These numbers are now consistent with the plots in Figure 5.

Page 7 lines 8-15. Once again, the values cited do not agree with the SSA values plotted in Figure 5.

This has been a typo that we have now corrected to 0.94 in agreement with Figure 5b. See also our reply to the previous comment.

Figure 6 presents the fraction of aerosol types observed at each site as function of month. The figure would be more informative if it gave the results in terms of the number of measurement rather than as a percentage. Thus, for example, one cannot appreciate the significance of the statement (page 7 line 24) "Pollution particles are detected most frequently at Seoul (67%)." I would suggest presenting the information like this:

This has been a very good suggestion. We have revised Figure 6 to include the distribution of aerosol types of the entire year. We have added information of the number of considered observations per month and year to provide further context for the fraction of aerosol types in %.

In general the figure captions are not very helpful. They should not just tell us what is being plotted, but also what one is expected to see in the plots.

We respectfully disagree with the Referee. Figure captions need to state what is being plotted (i.e. enable understanding of the figure) while their description and interpretation belongs into the text.

**Specific Criticisms**

Page 4 lines 18-19: The authors use Mexico City as a source of anthropogenic particles, that is, urban industrial aerosols. But as pointed out by Carabali et al. (10.1016/j.atmosres.2017.04.035), the Mexico City aerosol is dominated by two different types of aerosol, biomass burning and urban/industrial, depending on the season. (The burning of biomass by farmers in the hills surrounding the city is a major source of particulates.) It is not evident that the authors used the correct time frame for their presentation of Mexico City aerosols in Table 1 and Figure 7.

We thank the Referee for this comment. We did indeed miss to give a justification for our selection of sites. We have thus revised the beginning of the paragraph to: "*We follow earlier AERONET studies on aerosol classification (Dubovik et al., 2001; Gobbi et al., 2007; Giles et al., 2012) to select stations that are generally considered to be representative for …*"

We have looked at the paper by Carabali et al. (2017). They showed that the aerosol optical properties could be differed according to the season and it might be affected by different sources, i.e. anthropogenic or biomass burning. However, they conclude that the overall average of the Angstrom exponent (1.50) indicates the presence of fine particles at Mexico City. They also concluded that the bimodal structure of aerosol-size distribution at Mexico City resembles that found in some "other urban-industrial areas". The later indicates that anthropogenic sources dominate the local aerosol though it could be modulated by the presence of natural aerosols. They also concluded that aerosol absorption in Mexico City is close to AERONET retrievals in Beijing and Kanpur. This might be the reason why many studies treat the AERONET site Mexico City as urban-industrial.

Page 4 lines 24-26 and Figure 1. The authors state that the plots of SSA vs wavelength for different values of PLDR show "clearly distinguishable patterns." The figure is hard to read and the "pattern" is not really clearly distinguishable. The number of curves in each panel range from 7 to 9, making it hard to appreciate what the authors are trying to show. I would suggest that instead of 9 ranges of PLDR, the point could be made with 3 or 4 ranges. The authors say, "In addition, SSA at 1020 nm is remarkably different compared to SSA at other wavelengths according to the PLDR." (I think they mean "depending on" rather than "according to.") They go on to say, "Values are in the range between 0.91 and 0.94 for PLDR < 0.1 and between 0.96 and 0.99 for high PLDRs." This does not seem to me to be a significant difference since SSA can range from around 0.8 to 0.99. Finally, the different lines are different colors (representing different ranges of PLDR) but some of the colors are hard to tell apart. There are two shades of red and what appear to be two shades of black.

We have tidied up this figure. It now only shows SSA curves for four intervals of PLDR with clearly distinguishable colours. We have also revised the text based on the comments made by the two Referees.

There is one thing about Figure 1 that I find puzzling. Since the PLDR is used to evaluate the sphericity of the particles, it seems strange that it would be different at 440 nm than at, say, 1020 nm. Does this mean that the particles that respond most strongly at the shorter wavelengths have a different sphericity than the particles that respond most strongly at the larger wavelength? I would think that such an effect would be worth describing and explaining.

The literature on PLDR measurements at multiple wavelengths shows that the spectral behaviour of PLDR is indeed different for different aerosol types. This is because the effect depends on the size of the particles with respect to the measurement wavelengths. Particle shape becomes most important as particle size gets closer to the measurement wavelengths. Very non-spherical particles can basically be considered as spherical if they are very small compared to the used wavelength. We state in the text that we base our investigation on AERONET PLDRs at 1020 nm as those were found to closest resemble independent measurements with polarisation lidar.

Page 5 lines 3-10 and Figure 2. The figure shows the size distributions for the four East Asian sites. The caption should mention that the left column shows the fine mode and the right column shows the coarse mode and the vertical scales are different. Once again, the figure has far too many lines drawn on it, making it hard to understand.

We are sorry that this figure caused confusion. We have revised Figure 2 for better visibility. We now use the same vertical scale for fine and coarse mode. In addition, we only show four of the PLDR intervals in Figure 1. These are sufficient to visualise the change in the shape of the size distribution with PLDR. We hope that the revised figure is more suitable to transport the intended message.

**Minor Corrections**

Page 1 Line 19, "Radiative forcing of aerosols" should read "aerosol forcing by aerosols."

Changed to: "*Radiative forcing is …*"

Page 3 line 14," https://aeronet.gsfc.nasa.gov/.last access: 30 January2019 " I assume the words ".last access…2019" are a typo.

According to Copernicus guidelines, links to websites have to be provided with an access date. We state the date when we had last accessed the AERONET website before submitting the manuscript. Nevertheless, we have changed this part to "*accessed on 30 January 2019*"

Page 4 lines 1 and 2: The authors define the "Dust Ratio" R d in terms of δ nd and δ d . In equation (3) there is also a δ with no subscript which is undefined, unless it is the δ defined in equation (1). They then state that, "We used values of δ nd =0.02 and δ d =0.30 for pure dust for Asian dust." I don't know what the authors mean by "pure dust for Asian dust." Perhaps they mean "for pure dust and for Asian dust."

We are indeed referring to the δ defined in Eq. (1). The other part of this issue is a typo. The statement should have been "*for pure Asian dust*". This has been corrected.

Page 4 line 3, "The spectral SSA is the ratio of the scattering and extinction of light…"

This is not the correct definition of SSA.

To clarify, we have rephrased this statement to: "*The SSA is the ratio of the aerosol scattering coefficient to the aerosol extinction coefficient*"

Page 5 line 18. The word "study" should be deleted.

Done.

Page 10 line 9, Referring to Figure 7. “The SSA for NA is higher than SSA at the anthropogenic sites at all wavelengths.” According to Figure 7, this is not true at 440 nm. (The thin green curve and the thick green curve are not easily distinguishable.)

The Referee is correct. The statement has been revised to: “*The SSA for NA is higher than SSA at the anthropogenic sites at all wavelengths except for the observation at GSFC at 440 nm*.”

In addition, we have changed the colours used in this plot to provide better contrast between the different observations.

Page 10 line13. “Anthropogenic sites contain…” I think the authors meant to say “Biomass burning sites contain…”

Corrected.

Page 10 lines 16-17. “Finally, the spectral SSA of SA resembles the findings at Mongu…We note that the SSA of SA and Mongu are different.” Isn’t this a contradiction?

The Referee is correct. The statement has been changed to: “*Finally, the spectral SSA of SA is closest to the observations at Mongu…*”

Page 10 line 27. “Fine-mode particles contribute strongest to the …” should read, ”Fine-mode particles contribute most strongly to the …”

We have changed the statement as recommended.

**Anonymous Referee #2**

This paper attempts to determine the "aerosol-type" based upon the retrievals in the AERONET database. The main aerosol types defined in this paper are Pollution, Pollution-Dominated Mixtures (PDM), Dust-Dominated Mixtures (DDM), and Pure Dust (PD). Additionally, Pollution aerosols are divided further into four more subtypes, defined as Non-Absorbing (NA), Weakly Absorbing (WA), Moderately Absorbing (MA), and Strongly Absorbing (SA).

The main aerosol types are determined exclusively by the linear depolarization ratio (PLDR) at 1020 nm provided in the AERONET database. The pollution subtypes are determined exclusively by the single-scatter albedo (SSA) at 1020 nm.

The paper is well written and provides the reader with a relatively simple way of categorizing aerosols by type, but the paper would be much stronger if additional details

We thank the Referee for this positive assessment.

**Major issues:**

Page 2, Line 32: There are actually quite a few polarization lidars collocated with AERONET... see https://mplnet.gsfc.nasa.gov/. All MPLNETs are collocated with AERONET, since the AOT constraint provided by AERONET is necessary for the MPLNET extinction profile retrievals. Granted, it is difficult (impossible?) to do meaningful statistical studies with the data because one can only download one day of MPLNET data at a time, but the hardware has been in place for many years.

Thank you for this comment. We have elaborated our statement by adding: "*, i.e. well-calibrated polarisation-sensitive micro-pulse lidar or aerosol polarisation lidar*"

Page 3, line 13: Dubovik (2006) is an article about incorporating spheroids into the retrieval, and is not the appropriate citation in this context. The authors should cite these papers instead:

Dubovik, O. and King, M.: A flexible inversion algorithm for retrieval of aerosol optical properties from sun and sky radiance measurements, J. Geophys. Res., 105, 20673-20696, 2000.

Dubovik, O., Smirnov, A., Holben, B., King, M., Kaufman, Y., Eck, T., and Slutsker, I.: Accuracy assessments of aerosol optical properties retrieved from Aerosol Robotic Network (AERONET) sun and sky radiance measurements, J. Geophys. Res., 105, 9791-9806, 2000.

Thank you for the advice. The two papers have been added and cited here.

Page 3, Equation 3: I don't understand why the authors present this equation in the section entitled "Parameters", as they never really use it and it never shows up in plots or the discussion. They do state in Section 2.4 (page 5, line 15) that they are using R_d to define PLDR thresholds, and they provide a mapping between PLDR and R_d on lines 32-35 of page 5. However, the definitions of Pollution, PDM, DDM, and dust are rather arbitrary for both parameters.

I would just remove R_d from the paper altogether and define thresholds using the PLDR parameter. Alternatively, move Eq 3 into Sect 2.4 where there is some discussion of how this parameter is used, which would provide some context for the Equation... and then omit PLDR from the remainder of the paper and use R_d in the figures and discussion.

These are very good recommendations that we have implemented in the revised manuscript. We kept Eq. (3) as it provides an easy connection between PLDR and the amount of non-spherical particles but we followed the Referee's suggestion and moved the description of R_d. However, we thought it better to place it at the end of Section 2.3 rather than into Section 2.4 as recommended. We have changed Figure 4 to show R_d over FMF and have changed the text to focus on R_d rather than PLDR as suggested by the Referee.

Page 3, line 26: "Shin et al (2018) recently discussed..." Some context needs to be provided here... why are PLDR(870) and PLDR(1020) more reliable than PLDR(440) or PLDR(675), when all of these PLDRS come from the same AERONET retrieval? I believe that the authors came to this conclusion because the AERONET PLDR values at visible wavelengths were biased low of lidar measurements at 532 nm, whereas the near-infrared AERONET PLDRS had higher values that were more consistent with the lidar values at 532 nm. Some discussion here would strengthen the choice of PLDR(1020).

We have added a corresponding statement: "*The authors based this finding on comparison to literature values obtained from lidar observations of pure dust particles* ***which shows that AERONET-derived PLDRs at lower wavelengths are systematically lower than lidar observations at 532 nm.***"

Page 4, line 12 and elsewhere: There is not "Gosan" AERONET site... do the authors mean "Gosan SNU?"

Yes we do. Gosan has been changed to Gosan_SNU throughout the manuscript.

Page 4, line 31: Authors state: "The composition of mineral dust often includes clay minerals or iron oxides that lead to strong light-absorption at short wavelengths"

Although iron oxides are highly absorbing, clay minerals are not.

The reference to clay mineral has been removed.

Page 4, line 34: Authors state: "Aerosol particles which are categorized by PLDR into dust particles and pollution particles thus are relatively low light-absorbing at 440 nm compared to their light-absorbing capacity at other wavelengths."

I don't understand this logic... the authors just stated on lines 30-32 that "dust often contains... iron oxides that lead to strong light-absorption at short wavelengths." Also, authors mention biomass-burning on line 28, which also has strong light absorption at 440nm. So the authors contradict themselves.

We are sorry for the confusing and incorrect statement. The last sentence of this paragraph has not been correct. We have revised it to: "*Cases with considerable contribution of mineral dust as identified by high PLDR values therefore show relatively low SSA at 440nm compared to longer wavelengths.*"

Page 5, lines 3-6: Fig 2 does not show these concepts very well... the fine and coarse modes have different vertical axes, which makes it difficult to verify these words with the figure. There are also too many lines that are crossing all over the place, which makes it hard to understand. Since you are really discussing CMFvc vs PLDR, why not just plot these parameters as a scatter plot?

We agree that the figure has been too busy to understand easily. We have now changed it to show a single linear y-axis. We have also reduced the number of considered PLDR intervals. This makes for a tidier figure that still shows the change in size distribution for different intervals of PLDR, i.e. levels of dust contribution. We would like to keep the figure focussed on the actual size distributions as CMFvc vs PLDR would be very similar to FMF vs R_d in figure 4.

Page 5, line 8-9: Authors state: "External mixtures of mineral dust and non-spherical particles reveal PLDRs in the range from 0.08 to 0.30." What is the basis of this statement? Was this shown in Burton 2012 or Shin 2015? As written, it does not make sense. Dust is non-spherical, so you're discussing mixtures of non-spherical dust with other non-spherical aerosols? It is important to be clear on this point because you are using PLDR to define thresholds for PDM and DDM. However, here you define dust mixtures as 0.08 < PLDR < 0.28, but everywhere else the lower threshold for PDM is 0.06 (not 0.08)... why the inconsistency?

The difference in the range is due to the different wavelength. The statement refers to lidar measurements at 532 nm. We now mention that the values refer to that wavelength. We have also added references regarding the basis of this statement, i.e. Tesche et al. (2009, 2011) and Gross et al. (2011).

Page 5, line 18: Authors state: "The reason for using PLDR instead of FMF, which has been used, e.g. in Schuster et al. (2006) and Lee et al. (2010), is that the former study provides a clearer separation between non-spherical dust particles and rather spherical non-dust particles."

This statement needs to be backed up with data, as it seems contrary to Figure 4 and page 6, line 24, which states: "We find a strong negative correlation of R^2 = 0.80 for FMF vs. PLDR."

Thus, the data presented in this paper indicates that both FMF and PLDR are capable of discriminating dust from pollution. No case has been made that one of these parameters is significantly better than the other.

We agree that our statement has not been clear. We wanted to emphasize that PLDR and R_d are sensitive to particle shape. This allows for a direct detection of non-spherical dust particles without having to assume that dust particles are confined to the coarse mode. FMF can only be used as a proxy for the contribution of mineral dust as long as the coarse mode is made up exclusively of dust particles. Figure 4 shows a large number of cases with FMF>0.4 (the threshold for mineral dust in *Lee et al.*, 2010) that reveal R_d of 0.6 and higher. While mineral dust particles are generally considered as both large in size and non-spherical in shape, we believe that shape is a better indicator for mineral dust than size. This is also the rationale behind the statement the Referee addresses in the next comment, i.e. the reference to Shin et al. (2019) regarding the comparison of coarse-mode AOD and PLDR-derived dust AOD.

We have elaborated out statement and hope that the issue is now better addressed. We now state: "*The reason for using R_d instead of FMF, which has been used, e.g. in Schuster et al. (2006) and Lee et al. (2010), is that the former provides a clearer separation between dust and non-dust particles. The sensitivity of R_d to particle shape allows for a straightforward and size independent identification of non-spherical dust particles in a mixture while it has to*

*be assumed that dust is constrained to the coarse mode when using FMF for aerosol classification. However, dust might also be present in the fine mode (Mamouri and Ansmann, 2014, 2017).*"

Page 5, line 20: Authors state "Shin et al. (2019) compared coarse-mode AOD provided by AERONET to dust AOD retrieved with the use of PLDR and showed that the former tends to overestimate the contribution of mineral dust to AOD."

This sentence needs to be expanded, as it is unclear. First, what is being used as the "truth?" Are the authors assuming that their use of PLDR with the thresholds that they have chosen are the "truth?"

The statement refers to our earlier study in which we have adapted the PLDR-based aerosol-type separation of Tesche et al. (2009) to derive the contribution of mineral dust to AOD. The approach is based rather conservative PLDR thresholds for pure mineral dust and non-dust aerosols. We cannot know if this dust-related AOD is actually the truth. But we know that dust is not always confined exclusively to the coarse mode which is the basic assumption of using FMF as dust proxy. We can therefore state that separating the contributions of non-spherical and spherical particles based on parameters that are sensitive to particle shape is more meaningful for separating between dust, pollution, and their mixtures than using FMF. We hope that this rationale is now easier to understand based on the statement added in the reply to the previous comment.

Page 6, line 9: Authors state: " The SSA values for aerosol mixtures (e.g., BC with sulphate) vary, depending on the relative humidity and mixing ratio (e.g., 0.91 at 70% RH and 0.5 BC/sulphate mixing ratio for an internal mixture) (Wang and Martin, 2007)."

Check this... SSA = 0.91 is way too high of a value for a 0.5 BC/sulphate mixing ratio and is inconsistent with Wang and Martin (2007), Figure 3.

The Referee is correct. The mixing ratio we are referring to should have been 0.05 which corresponds to a SSA of 0.89 at 70% RH in Figure 3 of *Wang and Martin* (2007). The statement has been revised accordingly.

Page 6, line 12: Authors state: "The biomass-burning aerosol contains BC, while anthropogenic aerosol contains BC and/or NA."

This sentence implies that biomass-burning (BB) aerosols do not contain non-absorbing aerosols (NA), which is not true. Also, BB aerosols often contain BrC that is highly absorbing at 440 nm but non-absorbing at 1020 nm.

We are sorry for the confusing statement. We realised that it is not properly transporting the intended message. The statement has been revised to: "*We note that spherical non-dust particles which were classified by PLDR could contain either biomass-burning aerosol, anthropogenic aerosols, or both. For simplicity and because AODs during purely marine conditions are generally too low to yield the AERONET level 2.0 inversion products used in this study, we refer to these particles as pollution. We now assume that pollution with higher SSA consist mostly of NA whereas particles with lower SSA indicate that NA is mixed with BC. For this reason, an SSA threshold of 0.95 is used to identify NA and to mark the upper limit for pollution aerosols. Depending on 1020-nm SSA, absorbing aerosols are then further divided into, and weakly absorbing (WA, SSA= 0.90−0.95), moderately absorbing (MA, SSA= 0.85−0.9), and strongly absorbing (SA, SSA< 0.85). For reference, biomass-burning aerosol*

*generally contains a larger fraction of BC (and often brown carbon as well) compared to anthropogenic aerosol (Washenfelder et al., 2015), and thus, is likely to fall into the more absorbing categories.*"

Page 6, line 15: The setting of the "typing thresholds," both for SSA and PLDR, is the weakest element of this paper. Although the values chosen are reasonable (e.g., strongly absorbing aerosols have SSA < 0.85, Moderate absorbing have SSA 0.85-0.9, weakly absorbing SSA = 0.9-0.95, and non-absorbing have SSA > 0.95), they are basically pulled out of thin air.

Other studies (e.g., Burton 2012) use histograms and Mahalanobis distances to map multiple optical properties to known aerosol types.

We are sorry for missing to provide reference to the origin of the threshold values. The ones for the dust ratio R_d are based on the lidar literature on aerosol-type separation based on measurements of the particle linear depolarisation ratio. Values have been transformed into R_d as suggested by the Referees. The threshold values of SSA have been adopted from the AERONET-based aerosol classification presented by *Lee et al.* (2010). For clarity, we have revised the statement indicated by the Referee to: "*Depending on 1020-nm SSA and adapting the threshold values of* Lee et al. (2010), *absorbing aerosols are then further divided into, and weakly absorbing (WA, SSA = 0.90–0.95), moderately absorbing (MA, SSA = 0.85–0.9), and strongly absorbing (SA, SSA < 0.85).*"

Page 7, line 13: Authors state: "SSA at 1020 nm varies around of 0.87 in Sectors D and F."

This is inconsistent with Fig 5b, as SSA = 0.87 is not even on the scale (i.e., y-axis ranges from 0.88-1.0).

Thank you for catching this mistake. It was  a typo that has now been corrected to 0.94 in agreement with Figure 5b.

Page 7, lines 16-17: Authors state: "We conclude that the FMF might be too ambiguous a parameter to distinguish aerosol types in mixed dust-pollution plumes. In contrast, PLDR is a more reliable parameter for aerosol type classification in which mineral dust is part of the aerosol."

This is not at all obvious from the author's presentation. In fact, the argument is rather circular. i.e., use PLDR to distinguish type, then use FMF to validate conclusions, then discount FMF as ambiguous. Also, the authors note above that FMF is highly correlated with PLDR (R^2 = 0.8), so the two parameters are not really independent.

We are sorry for the confusion caused by our line of reasoning. In the reply to earlier Referee comments, we have already elaborated on why we think that a parameter that is sensitive to particle shape (i.e. PLDR or R_d) is better suited to identify non-spherical mineral dust particles than a parameter that is related to particle size, i.e. FMF. There is a strong correlation between the two parameters as mineral dust is predominantly coarse-mode aerosol. FMF is no longer a suitable proxy for dust if dust particles are also present in the fine mode. However, shape-dependent properties would still be sensitive to these particles as has been shown, e. g. by *Mamouri and Ansmann* (2014; 2017) which we now cite in the paper. For clarity, we have revised the statement to: "*As in our earlier study (Shin et al., 2019), we conclude that FMF with its relation to particle size might be too ambiguous a parameter to distinguish aerosol types in mixed dust-pollution plumes. In contrast, PLDR and R_d are related to particle*

*shape, and thus, likely to be better suited and physically more meaningful for aerosol type classification in which mineral dust is part of the aerosol mixture.*"

Page 7, lines 24-31: The authors need to add 12-month averages to Fig 6 so that the reader can follow along. None of the numbers in this paragraph correspond to the figure; presumably these numbers are averages over all 12 months, but the authors do not state this.

Thank you for this advice. These numbers do indeed refer to the annual average. We have added a new bar to the plots in Figure 6 that gives the annual average. We have also double-checked that the numbers in the text agree with Figure 6 and state that values refer to the annual average. As recommended by the other Referee, we have added information of the number of considered observations per month and year to provide further context for the fraction of aerosol types in %.

Page 8, line 33: This isn't really validation, as the authors do not have measurements to provide them with the "truth." Rather, this is basically a continuation of Section 3.2, but for different source regions.

The Referee is correct, though the selected sites have been used in various studies to represent the respective aerosol types. We have replaced "validate" with "further test".

I think the authors should include the seasonal variability at some of the sites in this section, similar to Fig 6. For instance, the West Africa has seasonal biomass burning as well as seasonal dust cycles. This should show up nicely at Banizoumbou and other African sites with a stacked chart like Fig 6.

Following the Referee's suggestion, we have investigated the potential of resolving seasonal variations in aerosol type using our typing scheme. We can indeed resolve changes in the occurrence of different aerosol types over West Africa based on the AERONET measurements at Dakar and Banizoumbou. We have added a respective paragraph in the discussion of the dust sites. However, we don't think that an additional figure is needed to transport this message. The new text is: "*We have considered the AERONET sites Dakar and Banizoumbou to investigate if our methodology can be used to resolve the seasonal cycles of dust and biomass burning over West Africa (not shown). We find that the two sites are dominated by PD, DDM, and PDM but that the ratio of the three types varies with season. PD contributes strongest in spring (MAM, 71% at Dakar and 88% at Banizoumbou) and summer (JJA, 74% and 72%), goes down in autumn (SON, 55% and 63%), and has minimum contributions in winter (DJF, 37% and 49%). The decrease in PD comes with an increase in DDM from spring and summer to autumn and winter (Dakar: 25% in MAM, 21% in JJA, 40% in SON, and 45% in DJF; Banizoumbou: 11% in MAM, 23% in JJA, 36% in SON, and 40% in DJF). In addition, PDM has a maximum in winter (17% at Dakar and 10% at Banizoumbou) with values between 0% and 5% during the other seasons. Contributions of other aerosol types are negligible at the two sites throughout the year.*"

Figure 4: Why show PLDR instead of R_p (from Eq 3)? If R_p really does present the contribution of dust to the particle backscatter coefficient, it would be much more interesting to see R_p than PLDR in this figure. Besides, PLDR only provides 4 broad categories of dust/pollution mixtures (dust, dust-dominated mixtures, pollution-dominated mixtures, and pollution), whereas the R_p would provide much higher resolution.

Figure 4 and the respective discussion have been changed to focus on R_d (see reply to previous comment on use of PLDR vs R_d).

Figure 5: I still don't like the multi-scale y-axis. Maybe try a single log scale for y-axis, if a single linear scale does not work.

Colors are difficult to discriminate, even for the non-color blind. Color-blind people have no chance of understanding this figure. I would add symbols to the lines for those folks.

And you don't really need all those error bars... May show one or more "representative" Error bars.... or just state some representative values in the caption. What do the error bars mean, anyways? 1-sigma? 2-sigma? 1 SDOM? 2 SDOM?

We are sorry for providing such a confusing figure. The figure has been revised for better visibility. Specifically, we now use a single linear y-axis, have removed all error bars (they were 1 SDOM), added symbols in the SSA plot and changed the lines to solid and dashed black and gray. We hope that these changes will make the figure more accessible also for colour blind readers.

Table 2: Something wrong here... FMF ranges from 0.31 to 0.90, but AE only ranges from 0.5 to 0.65. AE = 0.52 and 0.60 for PDM regions D&F, and AE=0.65 for polluted region G. All of these values are inconsistent with the literature, where AE < 1 is often used for "pure" dust. At a minimum, the authors should provide some discussion as to why their polluted sector has such a low AE.

We thank the Referee for spotting these inconsistencies. We did indeed use the wrong values for AE and SSA in Table 2. We have now included the proper number and double-checked that all parameters are consistent. We are sorry for this mistake.

Table 3: This is a little messy to look at. You don't really need the number of cases for each aerosol type, since that is covered by the first numerical column and the percentages. If you get rid of the number of cases, you'll have one value (the percentage) for each aerosol type, and this will be a lot easier for the reader to process.

Alternatively, this table could be converted into a stacked bar chart of percentages (like Fig 6). One stacked bar for each site.

Thank you for spotting this. The table has been revised to now only show the total number of cases and the percentages for each aerosol type.

**Minor issues:**

Page 2, line 28: replace "non-spherical" with "spherical."

We have corrected the typo.

# Aerosol-type classification based on AERONET version 3 inversion products

Sung-Kyun Shin[1,2], Matthias Tesche[1,3], Youngmin Noh[4], and Detlef Müller[1]

[1]School of Physics, Astronomy and Mathematics, University of Hertfordshire, Hatfield, United Kingdom
[2]now at Department of Atmospheric Particulate Matter Research, Seoul Institute of Technology, Seoul, Republic of Korea
[3]now at Leipzig Institute for Meteorology, Leipzig University, Leipzig, Germany
[4]Department of Environmental Engineering, Pukyong National University, Busan, Republic of Korea

**Correspondence:** Youngmin Noh (nym@pknu.ac.kr)

**Abstract.** This study proposes an aerosol-type classification based on the particle linear depolarization ratio (PLDR) and single scattering albedo (SSA) provided in the AErosol RObotic NETwork (AERONET) version 3 level 2.0 inversion product. We compare our aerosol-type classification with an earlier method that uses fine-mode fraction (FMF) and SSA. Our new method allows for a refined classification of mineral dust that occurs as a mixture with other absorbing aerosols: pure dust (PD), dust-dominated mixed plume (DDM), and pollutant-dominated mixed plume (PDM). We test the aerosol classification at AERONET sites in East Asia that are frequently affected by mixtures of Asian dust and biomass-burning smoke or anthropogenic pollution. We find that East Asia is strongly affected by pollution particles with high occurrence frequencies of 50% to 67%. The distribution and types of pollution particles vary with location and season. The frequency of PD and dusty aerosol mixture (DDM+PDM) is slightly lower (34% to 49%) than pollution-dominated mixtures. Pure dust particles have been detected in only 1% of observations. This suggests that East Asian dust plumes generally exist in a mixture with pollution aerosols rather than in pure form. In this study, we have also considered data from selected AERONET sites that are representative of anthropogenic pollution, biomass-burning smoke, and mineral dust. We find that average aerosol properties obtained for aerosol types in our PLDR-SSA-based classification agree reasonably well with those obtained at AERONET sites representative for different aerosol types.

## 1 Introduction

Atmospheric aerosol particles play an essential role in the global climate system by affecting the Earth's radiation budget (*Stocker et al.*, 2013). Aerosol particles directly interact with solar and terrestrial radiation through absorption and scattering of radiation. Aerosols also can act as cloud condensation nuclei and ice nucleating particles whereby they alter cloud properties (i.e., cloud albedo, cloud lifetime) and lead to a change in precipitation efficiency (*Twomey*, 1974). Radiative forcing ~~of aerosols~~ is a useful parameter in quantifying the radiative effect of aerosols on climate change. Estimates of aerosol radiative forcing require information on the amount of aerosol loading as well as aerosol properties (*Bellouin et al.*, 2013). The sign and the magnitude of the aerosol radiative forcing depends on aerosol characteristics (*Stocker et al.*, 2013). Despite an unprecedented global coverage of atmospheric aerosol information, it is still a challenging task to assess the aerosol radiative effect accurately.

Atmospheric aerosols are difficult to characterize in time and space due to their short lifetime and geographically diverse sources and production mechanisms. Moreover, atmospheric aerosol particles from different natural and anthropogenic sources also frequently mix and undergo aging processes during transport, which influences optical and microphysical properties of the bulk aerosols. An improved discrimination of different aerosol types by observations, particularly from space, increases the accuracy of estimates of the aerosol radiative impact and is important for the assessment of aerosol dispersion modelling (*Satheesh and Moorthy*, 2005).

Aerosol properties inferred from remote sensing measurements can be used to classify different aerosol types. Aerosol optical depth (AOD) and its spectral dependence which can be characterized by the Ångström exponent ~~(AE)~~ are typically used for aerosol classification from passive remote sensing observations. These parameters, together with the fine or coarse mode fraction of the aerosol size distribution, allow for a quantification of aerosol loading and aerosol size (*Schuster et al.*, 2006). Dominant aerosol types can then be inferred by using additional information on, e.g. possible source regions or transport pathways (*Boselli et al.*, 2012; *Shin et al.*, 2019). The use of spectral absorbing characteristics of aerosols add additional information on particle type (*Giles et al.*, 2012). For instance, *Kim et al.* (2007) used the fine mode fraction (FMF) from the MoDerate resolution Imaging Spectrometer (MODIS) to determine particle size and then used the aerosol index (AI) from the ozone monitoring instrument (OMI) to determine the light-absorbing characteristics of aerosols. Other studies have proposed to use properties related to particle size and absorption to determine the dominant aerosol type, based on AErosol RObotic Network (AERONET, *Holben et al.* 1998) observations (*Lee et al.*, 2010; *Russell et al.*, 2010; *Giles et al.*, 2012). AERONET provides a global, long-term aerosol data set that includes spectral AOD, complex refractive index, particle size distribution, single scattering albedo (SSA), and absorption aerosol optical depth ~~(AAOD)~~. The information on particle size and light-absorbing properties enables the identification of major aerosol types such as mineral dust, anthropogenic pollution, biomass burning smoke, and mixtures of aerosol particles. *Lee et al.* (2010) used SSA at 440 nm and FMF of AOD at 550 nm from AERONET to determine the absorbing properties and dominant size-mode of particles (i.e. fine or coarse mode) for aerosol classification. *Russell et al.* (2010) classified aerosol types based on the Absorption Ångström exponent ~~(AAE)~~. *Giles et al.* (2012) used SSA, ~~AAE, AE,~~ **Absorption Ångström exponent, Ångström exponent,** and FMF from AERONET to infer dominant aerosol types. More detailed and quantitative information useful for aerosol classification can be obtained from active aerosol remote sensing with lidar, particularly when we include information on the particle linear depolarization ratio (PLDR or $\delta^{\mathrm{p}}$) which is a very sensitive parameter with respect to particle shape (*Shin et al.*, 2019). Values of PLDR between 0.30 and 0.35 represent non-spherical particles (pure mineral dust, volcanic ash), while values close to zero indicate the presence of ~~non-~~spherical particles. Values in between these two extreme values characterize mixtures of spherical and non-spherical particles. Measurements of PLDR can be used to estimate the contribution of these two fundamentally different particle types (*Freudenthaler et al.*, 2009; *Tesche et al.*, 2009; *Burton et al.*, 2012, 2014, 2015; *Shin et al.*, 2015, 2019).

Several studies have determined aerosol types in which lidar-derived PLDR was combined with aerosol optical and microphysical properties inferred from AERONET observations (*Burton et al.*, 2012; *Russell et al.*, 2014). Although the combination of polarization lidar and AERONET observations might be an ideal option for aerosol classification, there are few AERONET

stations that are equipped with this additional instrumentation**, i.e. well-calibrated polarisation-sensitive micro-pulse lidar or aerosol polarisation lidar**.

Version 3 of the AERONET retrieval methodology provides us with spectral PLDR as standard inversion product. In this study, we use the information on the shape (PLDR) and light-absorbing properties (SSA) of particles for refining aerosol typing that can be obtained from using standard AERONET measurements. We retrieve the dominant aerosol type at selected AERONET sites in East Asia and investigate their seasonal variation and optical properties.

We describe our methodology in Section 2. In Section 3, we present and discuss our results. A summary and conclusion of this work is presented in Section 4.

## 2 Data and methodology

### 2.1 Parameters

Polarization lidar allows us to infer PLDR from measurements of the particle backscatter coefficient ($\beta_\lambda^{\mathrm{p}}$) in different planes of polarization compared to the plane of polarization of the emitted linearly polarized laser light:

$$\delta^{\mathrm{p}} = \frac{\beta^{\mathrm{p},\perp}}{\beta^{\mathrm{p},\parallel}}. \tag{1}$$

AERONET instruments measure direct solar radiation and sky radiation. The measurements are automatically analyzed using the AERONET inversion algorithm (*Dubovik and King*, 2000; *Dubovik et al.*, 2000b). The retrieved aerosol products are stored in the AERONET data base (https://aeronet.gsfc.nasa.gov/, ~~last~~ access**ed on**~~:~~ 30 January 2019). In the AERONET retrieval, the elements $F_{11}(\lambda)$ and $F_{22}(\lambda)$ of the Müller scattering matrix (*Bohren and Huffman*, 1983) are computed from the particle size distribution and the complex refractive index that can be inferred from AERONET **version 3** level 2**.0** data products. The element $F_{11}(\lambda)$ is proportional to the flux of scattered light in the case of unpolarized incident light while $F_{22}(\lambda)$ strongly depends on the angular and spectral distribution of the radiative intensity (*Bohren and Huffman*, 1983). From the elements $F_{11}(\lambda)$ and $F_{22}(\lambda)$ at the scattering angle 180°, $\delta^{\mathrm{p}}$ is computed as

$$\delta_\lambda^{\mathrm{p}} = \frac{1 - F_{22}(\lambda, 180°)/F_{11}(\lambda, 180°)}{1 + F_{22}(\lambda, 180°)/F_{11}(\lambda, 180°)}. \tag{2}$$

**AERONET version 3 level 2.0 inversion products include PLDRs and lidar ratios at 440, 670, 870, and 1020 nm. The parameter sphericity, which was provided in the AERONET version 2 inversion product, has been discontinued in version 3. We hence base this study on PLDR. This approach has the additional advantage that PLDR can also be obtained from independent measurements, e.g. with aerosol lidar.** *Noh et al.* (2017) report that PLDR from the AERONET inversion products shows high correlation with lidar-derived values. ~~PLDR can be used to calculate the contribution of dust to the particle backscatter coefficient for an external aerosol mixture. *Shimizu et al.* (2004) and *Tesche et al.* (2009) define the dust ratio ($R_{\mathrm{d}}$) as:~~

$$R_{\mathrm{d}} = \frac{(\delta^{\mathrm{p}} - \delta_{\mathrm{nd}}^{\mathrm{p}})(1 + \delta_{\mathrm{d}}^{\mathrm{p}})}{(\delta_{\mathrm{d}}^{\mathrm{p}} - \delta_{\mathrm{nd}}^{\mathrm{p}})(1 + \delta^{\mathrm{p}})}. \tag{3}$$

~~Here, $\delta_{nd}^{p}$ and $\delta_{d}^{p}$ indicate the PLDR of non-dust and pure dust particles, respectively. The corresponding values can be determined from lidar or AERONET observations (*Burton et al.*, 2014; *Burton et al.*, 2018).~~ *Shin et al.* (2018) ~~recently~~ discussed AERONET-retrieved PLDR from different source regions. The authors find that PLDRs at 870 and 1020 nm are likely to be the two most reliable quantities. The authors based this finding on comparison to literature values obtained from lidar observations of pure dust particles **which shows that AERONET-derived PLDRs at lower wavelengths are systematically lower than lidar observations at 532 nm**. ~~We accordingly apply the aerosol classification procedure to AERONET measurements at 1020 nm. We used values of $\delta_{nd}^{p} = 0.02$ and $\delta_{d}^{p} = 0.30$ for pure dust for Asian dust (*Shin et al.*, 2018). When PLDR was lower than $\delta_{nd}^{p}$ or higher than $\delta_{d}^{p}$, $R_d$ was set to 0 or 1, respectively.~~

The ~~spectral~~ SSA is the ratio of the **aerosol** scattering **coefficient** ~~and~~ **to the aerosol** extinction **coefficient** ~~of light by particles~~ and is generally used to define their absorbing characteristics. In this study, we **follow *Lee et al.* (2010) and** use SSA to distinguish between non-dust particles that are non-absorbing (NA), weakly absorbing (WA), moderately absorbing (MA), and strongly absorbing (SA).

### 2.2 Data selection

We selected AERONET sites in East Asia to develop our methodology. These sites are in a region that is influenced by both natural and anthropogenic aerosols such as anthropogenic particles from fossil fuel combustion, biomass-burning smoke, and mineral dust (*Nakata et al.*, 2016). We combine the stations Beijing and Xianghe into what we denote as Greater Beijing. The stations Seoul and Yonsei_University are considered representative for Seoul. Osaka is represented by the stations Osaka and Shirahama. We considered Gosan**_SNU** to represent regional background aerosols in East Asia as there are few anthropogenic sources near this site. The AERONET inversion is only performed for measurements with a 440-nm AOD larger than 0.4 (*Dubovik et al.*, 2006). For the aerosol-type classification we use the AERONET level 2.0 version 3 inversion products of particle size distribution, PLDR, and SSA available as of February 2018. This means that the time series considered here cover the time frame from the beginning of measurements at the respective sites up to between the end of 2016 and the middle of 2017.

We considered other AERONET stations to evaluate the results of our aerosol classification. **We followed earlier AERONET studies on aerosol classification (*Dubovik et al.*, 2001; *Gobbi et al.*, 2007; *Giles et al.*, 2012) to select** ~~These~~ stations **that** are generally considered to be representative for (1) anthropogenic particles: Goddard Space Flight Centre (GSFC, USA), Ispra (Italy), and Mexico City (Mexico), (2) biomass-burning smoke: Alta Floresta (Brazil), Mongu (Zambia), and Abracos Hill (Brazil), and (3) Saharan dust: Capo Verde (Cape Verde), Banizoumbou (Niger), and Dakar (Senegal). Detailed information on the AERONET sites considered in this study is provided in Table 1.

### 2.3 Correlation between PLDR and other ~~optical~~ properties

To investigate whether PLDR can be used as the base parameter for aerosol-type classification we analyzed how SSA and volume particle size distribution vary with respect to different intervals of PLDR. These parameters have been used for aerosol-type classification in previous studies (*Kim et al.*, 2007; *Lee et al.*, 2010). Figure 1 shows clearly distinguishable patterns of

spectral SSA **for different intervals of PLDR**. The increase of SSA with increasing wavelength for PLDR$> 0.28$ is characteristic for mineral dust (*Giles et al.*, 2012). In contrast, the decrease of SSA with increasing wavelength for PLDR$< 0.10$ is in line with anthropogenic pollution and biomass-burning smoke (*Giles et al.*, 2012). In addition, SSA at 1020 nm **shows the biggest range of values for different PLDR intervals** ~~is remarkably different compared to SSA at other wavelengths according to the PLDR~~. Values are in the range between 0.91 and 0.95 for PLDR$< 0.1$ and between 0.96 and 0.99 for high**er** PLDRs. In **comparison** ~~contrast to the other wavelengths~~, these differences are very small at 440 nm. The composition of mineral dust often includes ~~clay minerals or~~ iron oxides that lead to strong light-absorption at short wavelengths (*Derimian et al.*, 2008). The main light-absorber of anthropogenic pollution is black carbon or soot, which exhibits light absorption throughout the entire solar spectrum (*Bergstrom et al.*, 2002). **Cases with considerable contribution of mineral dust as identified by high PLDR values therefore show relatively low SSA at 440 nm compared to longer wavelengths.** ~~Aerosol particles which are categorized by PLDR into dust particles and pollution particles thus are relatively low light-absorbing at 440 nm compared to their light-absorbing capacity at other wavelengths.~~

Figure 2 shows that the variation of the fine-mode and the coarse-mode part of the size distribution with respect to PLDR is also clearly distinguishable. The fine-mode particles dominate at lower PLDR and their contribution decreases with increasing PLDR. Conversely, the contribution of the coarse-mode to the total volume concentration ~~(CMFvc)~~ increases as PLDR increases. ~~CMFvc~~ **It** is less than 0.5 for PLDR$< 0.06$ and higher than 0.9 for PLDR$> 0.30$.

**We know from lidar measurements at 532 nm that v**~~V~~alues of PLDR$\geq 0.3$ indicate nearly pure dust particles (*Freudenthaler et al.*, 2009; *Shin et al.*, 2018), whereas PLDR$< 0.08$ is representative for **marine aerosols,** anthropogenic pollution or **fresh** biomass-burning smoke (*Burton et al.*, 2012). External mixtures of mineral dust and non-spherical particles reveal **532-nm** PLDRs in the range from 0.08 to 0.30 (***Tesche et al.*, 2009, 2011; *Gross et al.*, 2011**). Consequently, ~~PLDR varies according to the dominant aerosol type in the mixture (*Shin et al.*, 2015).~~ **PLDR can be used to calculate the contribution of dust to the particle backscatter coefficient for an external aerosol mixture. *Shimizu et al.* (2004) and *Tesche et al.* (2009) used polarisation lidar measurements to define the dust ratio ($R_\mathrm{d}$) as:**

$$R_\mathrm{d} = \frac{(\delta^\mathrm{p} - \delta^\mathrm{p}_\mathrm{nd})(1+\delta^\mathrm{p}_\mathrm{d})}{(\delta^\mathrm{p}_\mathrm{d} - \delta^\mathrm{p}_\mathrm{nd})(1+\delta^\mathrm{p})}. \tag{4}$$

**Here, $\delta^\mathrm{p}_\mathrm{nd}$ and $\delta^\mathrm{p}_\mathrm{d}$ indicate the PLDR of non-dust and pure dust particles, respectively. The corresponding values can be determined from lidar or AERONET observations (*Burton et al.*, 2014; *Shin et al.*, 2018). We apply the $R_d$-retrieval to AERONET measurements at 1020 nm. We use values of $\delta^\mathrm{p}_\mathrm{nd} = 0.02$ and $\delta^\mathrm{p}_\mathrm{d} = 0.30$ for pure ~~dust for~~ Asian dust (*Shin et al.*, 2018). When PLDR is lower than $\delta^\mathrm{p}_\mathrm{nd}$ or higher than $\delta^\mathrm{p}_\mathrm{d}$, $R_\mathrm{d}$ it is set to 0 or 1, respectively.**

### 2.4 Aerosol classification method

Atmospheric aerosols are typically classified into four major types according to their size and light-absorbing property. For instance, *Lee et al.* (2010) used FMF and SSA from the AERONET version 2 level 2.0 inversion products to classify aerosols into black carbon (BC), mineral dust, non-absorbing (NA) particles, and mixed particles. In our aerosol classification method, we ~~use PLDR for obtaining information on the shape of the particles. We also use~~ **consider the contribution of non-spherical**

**particles (i.e., mineral dust) to the aerosol mixture based on thresholds of the dust ratio $R_{\mathrm{d}}$ as obtained from the shape-dependent parameter PLDR** ~~to set a threshold of PLDR for aerosol classification with respect to the contribution of mineral dust to the aerosol mixture.~~ **and use** SSA ~~is used~~ to distinguish absorbing from non-absorbing aerosols. The reason for using ~~PLDR~~ $R_{\mathbf{d}}$ instead of FMF, which has been used, e.g. in *Schuster et al.* (2006) and *Lee et al.* (2010), is that the former ~~study~~ provides a clearer separation between ~~non-spherical~~ dust ~~particles~~ and ~~rather spherical~~ non-dust particles. **The sensitivity of $R_{\mathbf{d}}$ to particle shape allows for a straightforward and size independent identification of non-spherical dust particles in a mixture while it has to be assumed that dust is constrained to the coarse mode when using FMF for aerosol classification. However, dust might also be present in the fine mode (*Mamouri and Ansmann*, 2014, 2017)**. *Lee et al.* (2010) used a threshold of FMF$< 0.4$ to identify mineral dust. *Jones and Christopher* (2007) reported annually mean values of MODIS FMF for mineral dust of $0.45 \pm 0.05$. *Shin et al.* (2019) compared coarse-mode AOD provided by AERONET to dust AOD retrieved with the use of PLDR and showed that the former tends to overestimate the contribution of mineral dust to AOD. As a consequence, FMF or fine-mode AOD, when used as proxy for identifying non-dust aerosols, would lead to a systematic underestimation of the contribution of non-dust particles to the total aerosol plume. Further benefits of using PLDR rather than FMF for aerosol type classification will be discussed later.

Figure 3 shows a flowchart of our aerosol classification method. The contribution of dust in the aerosol mixture is determined based on ~~using a~~ threshold**s of** $R_{\mathbf{d}}$ ~~for the PLDR~~. Previous studies reported **PLDR** values for Asian dust of 0.08 to 0.35 at 532 nm (*Murayama et al.*, 2004; *Shimizu et al.*, 2004; *Shin et al.*, 2015). Asian dust generally mixes with other aerosol types during long-range transport, which leads to a wide range in PLDR. *Shin et al.* (2015) used 0.08 at 532 nm as the threshold value to identify a contribution of mineral dust in mixed aerosol plumes. *Shimizu et al.* (2004) defined 0.1 at 532 nm as the threshold value for the classification of mixed mineral dust. In this study, we define pollution particles to show $R_{\mathbf{d}} < 0.17$ **(equivalent to 1020-nm** PLDR$< 0.06$**)** and mineral dust to show $R_{\mathbf{d}} > 0.89$ **(equivalent to 1020-nm** PLDR$> 0.28$**)**. Values between ~~0.06~~ **0.17** and ~~0.28~~ **0.89** are considered to represent mixtures of mineral dust and pollution aerosols. ~~Depending on~~ **We used a threshold of** $R_{\mathrm{d}} = 0.53$ **(equivalent to 1020-nm** PLDR$= 0.16$ ~~, we classified observations that fall into the range of PLDR between 0.06 and 0.28 as~~ **to further separate between** pollution-dominated mixed aerosol (PDM, $R_{\mathrm{d}} = 0.17 - 0.53$) and dust-dominated mixed aerosol (DDM, $R_{\mathrm{d}} = 0.53 - 0.89$). ~~PDM is characterized by PLDR between 0.06 and 0.16 while DDM is identified for PLDR between 0.16 and 0.28.~~ The light-absorbing properties and size of PDM is likely to be closer to the characteristics of pollution particles than to DDM. In the same way, the light absorbing properties and size for DDM are more likely to resemble the characteristics of pure dust.

SSA at 440 nm is usually used to identify dust particles (*Kim et al.*, 2007; *Lee et al.*, 2010). Here, we use SSA at 1020 nm as we have already classified mineral dust and non-dust particles based on ~~PLDR~~ $R_{\mathbf{d}}$. This means that we can make use of the better contrast that we find between black carbon and dust particles when using SSA at 1020 nm, and we can use this contrast for our threshold-based identification of different absorbing particle types and their mixtures. The SSA at 1020 nm of water soluble aerosols, including sulphates, is close to unity (*Hess et al.*, 1998), whereas SSA is close to zero for BC (0.07 at 1020 nm, *Haywood and Ramaswamy* 1998). The SSA values for aerosol mixtures (e.g., BC with sulphate) vary, depending on the relative humidity and mixing ratio (e.g., 0.**8**9~~1~~ at 70% RH and 0.**0**5 BC/sulphate mixing ratio for an internal mixture**, see Figure 3 in**

***Wang and Martin* (2007)**). *Dubovik et al.* (2002) report on SSA at 1020 nm of 0.83-0.95, 0.78-0.91, 0.97-0.99, and 0.97 for urban/industrial pollutant, biomass burning, desert dust, and marine aerosol, respectively. ~~We note that pollution particles which were classified by PLDR $R_{\mathbf{d}}$ could consist of both biomass-burning aerosol and anthropogenic aerosols. The biomass-burning aerosol contains BC, while anthropogenic aerosol contains BC and/or NA. Therefore, we conclude that anthropogenic aerosols with higher SSA consist mostly of NA whereas particles with lower SSA indicate that NA is mixed with BC. For this reason, an SSA threshold of 0.95 is used to identify NA and to mark the upper limit for SSA of anthropogenic pollution. Depending on 1020-nm SSA, absorbing aerosols are then further divided into strongly absorbing (SA, SSA$< 0.85$), moderately absorbing (MA, SSA$= 0.85 - 0.9$), and weakly absorbing (WA, SSA$= 0.90 - 0.95$).~~ **We note that spherical non-dust particles which were classified by $R_{\mathbf{d}}$ could contain either biomass-burning aerosol, anthropogenic aerosols, or both. For simplicity and because AODs during purely marine conditions are generally too low to yield the AERONET level 2.0 inversion products used in this study, we refer to these particles as pollution. We now assume that pollution with higher SSA consist mostly of NA whereas particles with lower SSA indicate that NA is mixed with BC. For this reason, an SSA threshold of 0.95 is used to identify NA and to mark the upper limit for pollution aerosols. Depending on 1020-nm SSA and adapting the threshold values of *Lee et al.* (2010), absorbing aerosols are then further divided into, and weakly absorbing (WA, SSA = 0.90–0.95), moderately absorbing (MA, SSA = 0.85–0.9), and strongly absorbing (SA, SSA < 0.85). For reference, biomass-burning aerosol generally contains a larger fraction of BC (and often brown carbon as well) compared to anthropogenic aerosol (*Washenfelder et al.*, 2015), and thus, is likely to fall into the more absorbing categories.**

## 3 Results

### 3.1 FMF versus ~~PLDR~~ $R_{\mathbf{d}}$ for aerosol-type classification

Figure 4 shows a 2-d histogram distribution of the relation between FMF and ~~PLDR~~ $R_{\mathbf{d}}$. Desert dust predominately consists of coarse-mode particles, whereas combustion-produced particles are predominantly found in the FMF of particle size distributions. **Nevertheless, non-spherical dust particles might also be present in the fine mode – in which case FMF would no longer be ideally suited to represent dust in the particle size distribution.** ~~The PLDR~~ $R_{\mathbf{d}}$ is close to zero for spherical particles such as anthropogenic or smoke particles and increases with increasing ~~particle non-sphericity~~ **dust contribution**. The dominant aerosol type in the aerosol mixture can be distinguished based on knowledge of FMF and ~~PLDR~~ $R_{\mathbf{d}}$ **as the parameters refer to particle size and shape, respectively**. We find a strong negative correlation of $R^2 = 0.77$ for FMF versus ~~PLDR~~ $R_{\mathbf{d}}$. The use of ~~PLDR~~ $R_{\mathbf{d}}$ **and FMF** allows us to separate between pure dust (PD, sector A), dust-dominated mixture (DDM, sectors B, C, and E), pollution-dominated mixture (PDM, sectors D and E), and pollution (sector G). This leads to an overall more comprehensive aerosol classification with respect to dusty mixtures.

Figure 5 shows the mean volume particle size distribution and SSA of the seven sectors. The optical and microphysical properties of the aerosols in each sector are listed in Table 2. The volume particle size distribution and SSA for the two dust sectors A and B are markedly different. Sector A shows a mean FMF of $0.31 \pm 0.18$ while this value increases to $0.41 \pm 0.17$

in sector B. Additionally, the SSA at 1020 nm in sector A is $0.99 \pm 0.01$ while SSA in Sector B drop to $0.97 \pm 0.01$. Although both Sectors C and D are classified as mixed aerosols, particle size distribution of Sector C is characterized by a more dominant coarse mode than particle size distribution in Sector D.

The difference in the values of optical and microphysical properties of aerosol in Sectors E, F, and G (pollution dominated) is even more pronounced. Values of FMF are $0.71 \pm 0.09$, $0.80 \pm 0.08$, and $0.90 \pm 0.05$, respectively. SSA is $0.96 \pm 0.01$, $0.94 \pm 0.01$, and $0.92 \pm 0.01$, respectively. The spectral dependence of SSA in Sector E is also distinguishable from that of SSA in Sectors F and G. SSA increases with increasing wavelength in sector E. Such a spectral behaviour is a characteristic feature of mineral dust. The SSA decreases with increasing wavelength in Sector G. We find little spectral variation of SSA in Sector F. Sectors F and G are more likely to represent pollution particles, whereas Sector E more likely contains mixtures of pollution and mineral dust.

The volume particle size distribution and spectral SSA in Sector A (pure dust based on PLDR) is clearly different from the ones in the other sectors. Sector A contains coarse-mode-dominated particle size distributions (FMF$= 0.31 \pm 0.18$) and shows a spectral SSA that resembles the one of mineral dust. Similarly, the spectral characteristics of SSA of aerosols in Sectors B, C, and E, which are classified as dust dominant mixtures, are characteristic for dust particles. However, SSA at 1020 nm is lower (0.96-0.97) compared to SSA at 1020 nm in Sector A. SSA at 1020 nm varies around ~~of~~ 0.94 in Sectors D and F. These sectors were classified as pollution-dominated mixtures (based on PLDR). The volume size distributions for Sectors D and F show that both coarse- and fine-mode particles are present in these mixtures. Sector G resembles the characteristics of pollution particles (high FMF and low SSA).

~~W~~ **As in our earlier study (*Shin et al.*, 2019), w**e conclude that FMF **with its relation to particle size** might be too ambiguous a parameter to distinguish aerosol types in mixed dust-pollution plumes. In contrast, PLDR **and $R_d$ are related to particle shape, and thus, likely to be better suited and physically more meaningful** ~~is a more reliable~~ parameter**s** for aerosol type classification in which mineral dust is part of the aerosol **mixture**. Our method is particularly useful for observations in East Asia were mineral dust is almost always mixed with pollution. We therefore propose a refined categorization into pure dust, dust-dominated mixtures, pollution-dominated mixtures, and pollution.

### 3.2 Characteristics of aerosol types over East Asia

We investigated the regional and seasonal characteristics of aerosol over East Asia. The rates of occurrences of aerosol types at each AERONET observation site are shown in Figure 6. Regardless of season, pollution particles (NA+WA+MA+SA) are detected persistently over East Asia with 51~~0~~%-66~~7~~% occurrence rate **when considering the annual average**. Pollution particles are detected most frequently at Seoul **and Osaka** (66~~7~~%). The lowest occurrence rate of pollution of 51~~0~~% was found at Gosan**_SNU**. The seasonal variation and specific type of pollution differ for the different sites. Aerosols classified as more light absorbing (MA+SA), are detected most frequently at Greater Beijing (SA: 4%, MA: 15%) and Osaka (SA: 5%, MA: 15%) followed by Seoul (SA: 2%, MA: 9%) and Gosan**_SNU** (SA: 3%, MA: 4%). The most frequently detected aerosol types over Seoul were NA (24%)**, PDM (28%),** and WA (32%). Differences in the frequency of different types of pollution particles, i.e. the BC-dominated types MA and SA and WA and NA which contain little or no BC, can be explained by the sources of the

aerosols. The occurrence rate of MA and SA at Greater Beijing (19%) is larger than at Seoul (11%). China has become a major source of BC because of fossil fuel combustion stemming from industry, domestic heating, and cooking. The contribution of BC in pollution thus has increased. In contrast, water-soluble (hygroscopic) aerosol particles such as sulphate or nitrate might be dominant in the anthropogenic pollution plumes over Seoul.

The occurrence rate of pure and polluted dust (PD, DDM, and PDM) over East Asia is slightly lower (34%-49%) than that of dust-free pollution. PDM is the most frequently detected aerosol type (over East Asia) of all types that include dust, i.e. PD, DDM, and PDM. The occurrence rates of PDM were 28%, 28%, 33%, and 23% for Greater Beijing, Seoul, Gosan**_SNU**, and Osaka, respectively. In contrast, the occurrence rate for PD was around 1% at most sites. The highest occurrence rate for PD is found at Greater Beijing (1%). Central Asian dust usually has traveled over densely populated and highly industrialized areas of China before it is detected. That means, as the result of transport path and time dust has usually mixed with pollutants before being detected (*Sun et al.*, 2005; *Shin et al.*, 2015). The lowest occurrence rate for PD and relatively higher occurrence rate for PDM and DDM over East Asia corroborates this assumption, i.e. that dust particles over East Asia are typically mixed with anthropogenic pollution **or that any stratification of the different aerosol types will show the optical signature of a mixture in the column-integrated AERONET measurements**.

The seasonal variation of each aerosol type retrieved with our aerosol classification method corroborates the findings of *Xia et al.* (2007), *Guo et al.* (2011), and *Jung et al.* (2009). Overall, dust-containing aerosol types (PD, DDM, and PDM) have the highest occurrence rates during spring with as much as 82% of cases for Gosan**_SNU** in April. This is in line with the Asian dust season in spring (*Guo et al.*, 2011). PD is observed at all sites during spring but only with low occurrence rates of 1% to 4%. PD is also rarely observed during the other seasons. The occurrence rates of pollutant particles are consistently high except during spring. The distributions and types of pollutant particles are rather complex because of the variety of their source with respect to location and season. Higher rates of SA and MA are detected at most observation sites during winter, which is likely the result of increased combustion of coal for domestic heating. In contrast, the Gosan**_SNU** site is less influenced by strong light-absorbing particles during winter compared to the other observation sites as it is located away from highly industrialized areas. The higher SA and MA occurrence rates detected during summer at Osaka might be due to regional climate effects: a high oxidant level from local emissions, high temperature, and strong thermal insulation support the conversion of volatile organic compounds into secondary organic aerosols (~~SOA,~~ *Sano et al.* 2016). The aged ~~SOA~~ **secondary organic aerosols** could produce brown carbon ~~(BrC)~~ which is significantly light-absorbing (*Liu et al.*, 2016).

Another feature to note is the occurrence rate of NA and WA which increases during summer at all sites. Sulphate and nitrate are major contributors to the aerosol loading during summer over East Asia. Strong solar radiation, high ambient temperature, and high relative humidity during summer in East Asia enhance photochemical processes. These conditions may have been responsible for the higher summer concentrations of ammonium sulphate and nitrate (*Jung et al.*, 2009). The Asian monsoon is another possible reason for the increased frequency of occurrence of NA and WA during summer. Increased relative humidity and associated hygroscopic particle growth during monsoon season can cause changes in aerosol scattering properties (*Xia et al.*, 2007). Regardless of season, significant amounts of NA and WA are detected at the coastal sites Gosan**_SNU** and

Osaka. The high valued of NA and WA might be the result of large contributions of maritime aerosol which is strongly light-scattering as well as highly hygroscopic.

### 3.3 Dominant aerosol types at representative aerosol source regions

In order to ~~validate~~ **further test** our method, we used it to determine the dominant aerosol types at well-characterized AERONET sites representative for anthropogenic pollution, biomass burning particles, and mineral dust (*Dubovik et al.*, 2002; *Giles et al.*, 2012; *Choi et al.*, 2016). Details on the selected sites together with the occurrence rates of different aerosol types are given in Table 3.

The dominant aerosol type at dust sites was PD with occurrence rates of 64% to 81%. PD was most frequently detected at Cape Verde with 81% occurrence rate. Additionally, notable occurrences rate for DDM (16% to 35%) and PDM (0% to 4%) are also found at the dust sites. This suggests that AERONET sites in or close to source regions of mineral dust are frequently affected by local pollution or other aerosols from sources upwind. The highest occurrence rate of 35% for mixed dust types (DDM+PDM) was found at Dakar where local pollution has a much stronger effect on aerosol composition compared to other Saharan sites (*Petzold et al.*, 2011). **We have considered the AERONET sites Dakar and Banizoumbou to investigate if our methodology can be used to resolve the seasonal cycles of dust and biomass burning over West Africa (not shown). We find that the two sites are dominated by PD, DDM, and PDM but that the ratio of the three types varies with season. PD contributes strongest in spring (MAM, 71% at Dakar and 88% at Banizoumbou) and summer (JJA, 74% and 72%), goes down in autumn (SON, 55% and 63%), and has minimum contributions in winter (DJF, 37% and 49%). The decrease in PD comes with an increase in DDM from spring and summer to autumn and winter (Dakar: 25% in MAM, 21% in JJA, 40% in SON, and 45% in DJF; Banizoumbou: 11% in MAM, 23% in JJA, 36% in SON, and 40% in DJF). In addition, PDM has a maximum in winter (17% at Dakar and 10% at Banizoumbou) with values between 0% and 5% during the other seasons. Contributions of other aerosol types are negligible at the two sites throughout the year.**

The sites for anthropogenic pollution show an extremely high occurrence rate of pollutants of 93% to 99%, though the occurrence rates of the individual sub-types vary from site to site. Higher occurrence rates of NA and WA were found at GSFC (34% and 47%) and Ispra (32% and 37%). Conversely, a higher occurrence rate of MA (34%) and SA (29%) was found at Mexico City, which is frequently affected by severe air pollution that mostly consists of fine-mode and carbonaceous aerosols (*Choi et al.*, 2016). *Choi et al.* (2016) used cluster analysis in combination with AERONET data and found that secondary inorganic particles dominate at GSFC. Carbonaceous aerosol has strong light-absorption properties, whereas secondary inorganic aerosols such as sulphates predominantly scatter light (*Bond and Bergstrom*, 2006).

The frequency distribution of SA and MA are higher at the biomass-burning sites. Those sites are considered to be affected by mostly light-absorbing particles from combustion. A high occurrence rate of 96% of SA was found at Mongu. MA is the most frequently detected type at Alta Floresta (42%) and Abracos Hill (41%). BC is produced by flaming fires, i.e. at high temperatures. This type of BC production is prevalent at Mongu, whereas production of primary organic carbon ~~(OC)~~ at lower temperature (smoldering fires) is dominant at Alta Floresta (*Reid et al.*, 2005; *Choi et al.*, 2016). The occurrence rates of NA

(4%) and WA (34) at Alta Floresta and Abracos Hill are also distinguishable from the rates at Mongu where less than 0.5% were detected as NA or WA. The photochemical formation of secondary inorganic aerosols due to emissions from biomass burning seems to be much more frequent at Alta Floresta and Abracos Hill compared to Mongu (*Choi et al.*, 2016).

Figure 7, analogous to Figures 1 and 2, presents the mean spectral SSA and volume particle size distributions for the AERONET sites that are mainly affected by anthropogenic pollution, biomass-burning smoke, and Saharan dust. The spectral behaviour of SSA at these sites strongly resembles the ones presented by *Dubovik et al.* (2002), *Eck et al.* (2009), *Giles et al.* (2012), and *Shin et al.* (2018). Dust particles exhibit strong light absorption at short wavelengths and lower absorption in the visible and near infrared wavelength region (*Shin et al.*, 2018). Fine-mode particles and hygroscopic particles such as sulphate show nearly neutral spectral dependence of SSA and overall stronger light-scattering, i.e. higher SSA (*Dubovik et al.*, 2002). BC has the strongest light-absorption properties in the near-infrared wavelength region. ~~OC and BrC~~ **Organic and brown carbon** exhibit stronger light-absorption properties at ultraviolet and visible wavelengths (*Eck et al.*, 2009).

The SSA at sites that represent anthropogenic pollution likely reflects the spectral features of SSA of fine-mode particles and hygroscopic particles. The value of SSA at Mexico City is lower than at other anthropogenic sites in the entire wavelengths. Mexico City is frequently influenced by air pollution that likely consists of more carbonaceous aerosols, whereas GSFC and Ispra are affected by secondary inorganic particles (*Choi et al.*, 2016). Additionally, the spectral dependence of SSA at the biomass-burning sites is similar to that of BC. We note that the values of SSA at the Mongu site are much lower than the values of SSA at the other biomass-burning sites in the entire wavelength. Various absorbing aerosols (e.g., ~~BC, OC, BrC~~**black, organic and brown carbon**, or secondary inorganic aerosols) can be emitted from biomass burning. The lower SSA at Mongu might be the result of a higher fraction of BC compared to the other biomass-burning sites. Consequently, the spectral dependence of SSA at Alta Floresta and Abracos Hill is more neutral with high values of SSA compared to Mongu. BC has the strongest light-absorption properties in the near-infrared wavelength region, while ~~OC and BrC~~ **organic and brown carbon** exhibit stronger light-absorption properties at ultraviolet and visible wavelengths (*Eck et al.*, 2009). The spectral dependence of SSA at the dust sites is representative of mineral dust particles.

Figure 7 also compares the spectral SSA at the AERONET sites to the spectral SSA of the aerosol types defined in our classification method (see Figure 3). The SSA for NA is higher than SSA at the anthropogenic sites at all wavelengths **except for the observation at GSFC at 440 nm**. The SSA for WA is similar to values obtained at GSFC and Ispra. We conclude from this that NA – in view of the definition of aerosol type – consists to a largest degree of light-scattering particles. Similarly, WA represents aerosols that contain both light-scattering and light-absorbing particles with the light-scattering contribution being predominant.

~~Anthropogenic~~ **Biomass-burning** sites ~~contain~~ **observe** light-scattering particles and light-absorbing particles, which is reflected in SSA. The spectral SSA of MA is similar to the values found at Alta Floresta and Abracos Hill except at the short wavelength. Consequently, MA is an aerosol mixture in which light-absorbing particles have a stronger impact. The absorbing properties are most likely related to the contribution of ~~OC~~ **organic carbon**. Finally, the spectral SSA of SA ~~resembles the findings~~ **is closest to the observations** at Mongu and suggests that the light- absorbing properties of SA are related to a strong contribution of BC. We note that the SSA of SA and Mongu are different. SA has been defined based on observations in East

Asia where absorbing particles are likely present in complex mixtures. In contrast, BC is considered as the dominant aerosol at Mongu.

The spectral SSA of DDM and PD is similar to the one found at the dust sites. However, the SSA of DDM is slightly lower than SSA of PD and of the AERONET dust sites as a result of mixing with pollutant particles. Accordingly, the SSA of PDM are even lower than of PD, DDM, and AERONET dust sites as it is defined to feature a larger contribution of pollutants.

The volume size distributions show a dominance of coarse-mode particles at the dust sites. Coarse-mode particles also contribute strongly to the total volume size distribution for PD and DDM, whereas a lower contribution of coarse-mode particles is found for PDM. This result is in line with an increased concentration of anthropogenic pollution or biomass-burning smoke which, in the PDM type, are typically considered to be fine-mode particles (*Eck et al.*, 1999).

Fine-mode particles contribute ~~strongest~~ **most strongly** to the total volume size distribution at biomass-burning sites. Additionally, the contribution of fine-mode and coarse-mode seems evenly distributed in the total volume size distribution for MA and SA. *Reid et al.* (1998) found from studies in rain forest regions of Brazil that fresh smoke particles are significantly smaller than well-aged smoke particles. We believe that fresh smoke particles contribute significantly at the biomass-burning sites, whereas MA and SA detected over East Asia are affected not only by fine-mode particles but also a considerable amount of coarse-mode particles, in contrast to the source regions of biomass burning. The contributions of fine-mode and coarse-mode particles to the total volume size distributions are rather similar for the anthropogenic sites. However the contribution of fine-mode particles to the total volume size distributions is dominant for NA.

## 4 Summary and conclusions

We presented a methodology that is used for classifying the dominant types of aerosol particles in mixed aerosol plumes. **Note that in the case of AERONET measurements, mixtures might also refer to a vertical stratification of different aerosol types that shows the column-integrated optical signature of a mixed plume.** We used PLDR and SSA that are provided in the AERONET version 3 level 2.0 inversion products. Dusty aerosol mixtures were separated according to pure dust, dust-dominated mixtures, pollution-dominated mixtures and pollution. The pollutants were classified as non-absorbing, weakly absorbing, moderately absorbing and strongly absorbing particles based on using SSA at 1020 nm. The new aerosol typing method provides detailed information on aerosol mixtures that contain varying levels of mineral dust.

We tested our method at East Asian AERONET sites that are frequently affected by various aerosol type. We found that aerosols categorized as pollutant (NA+WA+MA+SA) are most frequently detected over East Asia. The detection rate was 50%-67%. The distribution and types of pollutant vary according to the location of sites and season. The frequency distribution for PD or dust-containing aerosol (DDM+PDM) plumes is lower than that of pollutants. Moreover, PD was detected in less than 1% of the observations at most sites over East Asia. This suggests that dust over East Asia is almost always mixed with other types of aerosol.

We compared the results of our aerosol-type classification to the aerosol properties obtained from selected AERONET sites which are considered to be representative for different aerosol types, i.e. anthropogenic pollution, biomass-burning smoke and

mineral dust. For anthropogenic pollution, we found that that MA and SA occur most frequently at Mexico City, whereas GSFC and Ispra are affected most strongly by NA and WA. The frequency distribution of SA and MA is higher at the biomass-burning sites. Those sites are affected by mostly light-absorbing particles from combustion. PD is the dominant aerosol at dust sites. From the comparison to representative AERONET sites, we conclude that the method we use to identify dominant aerosol types over East Asia also leads to reasonable results at other sites. The proposed method has the potential to provide improved information on aerosol type in regions where various types of aerosol are frequently present in the form of complex mixtures – not only over East Asia but also elsewhere on the globe. Application of our aerosol-typing method to the global AERONET data base will provide useful information for the validation of chemical transport modelling as well as (active) spaceborne sensors that provide PLDR observations.

*Data availability.* The data used in this work are freely available through the AERONET portal at http://aeronet.gsfc.gov/.

*Author contributions.* SKS, MT, and YN had the idea for this study. SKS and MT performed the data analysis and prepared the figures. All authors contributed to the discussion of the findings and the preparation of the manuscript.

*Competing interests.* The authors declare that no competing interests are present.

*Acknowledgements.* We thank the principal investigators and their staff for establishing and maintaining the AERONET sites used in this investigation. This work was supported by a National Research Foundation of Korea (NRF) grant funded by the Korean government (NRF-2018R1D1A3B07048047).

## References


Bellouin, N., Quaas, J., Morcrette, J.-J., and Boucher, O.: Estimates of aerosol radiative forcing from the MACC re-analysis, Atmos. Chem. Phys., 13, 2045-2062, http://doi.org/ 10.5194/acp-13-2045-2013, 2013.

Bergstrom, R. W., Russell, P. B., and Hignett, P.: Wavelength dependence of the absorption of black carbon particles: Predictions and results from the TARFOX experiment and implications for the aerosol single scattering albedo, J. Atmos. Sci., 59, 568–578, 2002.

Bohren, C. and Huffman, D.: Absorbing and scattering of light by small particles. Wiley, https://doi.org/10.1002/9783527618156, 1983.

Bond, T. C. and Bergstrom, R. W.: Light absorption by carbonaceous particles: An investigative review, Aerosol Sci. Tech., 40, 27-67, https://doi.org/10.1080/02786820500421521, 2006.

Boselli, A., Caggiano, R., Cornacchia, C., Madonna, F., Mona, L., Macchiato, M., Pappalardo, G., and Trippetta, S.: Multi year sun-photometer measurements for aerosol characterization in a Central Mediterranean site, Atmos. Res., 104, 98-110, https://doi.org/10.1016/j.atmosres.2011.08.002, 2012.

Burton, S. P., Ferrare, R. A., Hostetler, C. A., Hair, J. W., Rogers, R. R., Obland, M. D., Butler, C. F., Cook, A. L., Harper, D. B., and Froyd, K. D.: Aerosol classification using airborne High Spectral Resolution Lidar measurements – methodology and examples, Atmos. Meas. Tech., 5, 73-98, https://doi.org/10.5194/amt-5-73-2012, 2012.

Burton, S. P., Vaughan, M. A., Ferrare, R. A., and Hostetler, C. A.: Separating mixtures of aerosol types in airborne High Spectral Resolution Lidar data, Atmos. Meas. Tech., 7, https://doi.org/10.5194/amt-7-419-2014, 2014.

Burton, S. P., Hair, J. W., Kahnert, M., Ferrare, R. A., Hostetler, C. A., Cook, A. L., Harper, D. B., Berkoff, T. A., Seaman, S. T., Collins, J. E., Fenn, M. A., and Rogers, R. R.: Observations of the spectral dependence of linear particle depolarization ratio of aerosols using NASA Langley airborne High Spectral Resolution Lidar, Atmos. Chem. Phys., 15, 13453-13473, https://doi.org/10.5194/acp-15-13453-2015, 2015.

Choi, Y., Ghim, Y. S., and Holben, B. N.: Identification of columnar aerosol types under high aerosol optical depth conditions for a single AERONET site in Korea. J. Geophys. Res., 121, 1264-1277, https://doi.org/10.1002/2015JD024115, 2016.

Derimian, Y., Karnieli, A., Kaufman, Y., Andreae, M., Andreae, T., Dubovik, O., Maenhaut, W., and Koren, I.: The role of iron and black carbon in aerosol light absorption, Atmos. Chem. Phys., 8, 3623-3637, https://doi.org/ 10.5194/acp-8-3623-2008, 2008.

Dubovik, O. and King, M.: A flexible inversion algorithm for retrieval of aerosol optical properties from sun and sky radiance measurements, J. Geophys. Res., 105, 20673-20696, 2000.

**Dubovik, O., Smirnov, A., Holben, B., King, M., Kaufman, Y., Eck, T., and Slutsker, I.: Accuracy assessments of aerosol optical properties retrieved from Aerosol Robotic Network (AERONET) sun and sky radiance measurements, J. Geophys. Res., 105, 9791-9806, 2000.**

**Dubovik, O., Holben, B., Eck, T. F., Smirnov, A., Kaufman, Y. J., King, M. D., Tanré, D., and Slutsker, I.: Variability of Absorption and Optical Properties of Key Aerosol Types Observed in Worldwide Locations, J. Atmos. Sci., 59, 590-608, https://doi.org/10.1175/1520-0469(2002)059<0590:VOAAOP>2.0.CO;2, 2002.**

**Dubovik, O., Holben, B., Eck, T. F., Smirnov, A., Kaufman, Y. J., King, M. D., Tanré, D., and Slutsker, I.: Variability of absorption and optical properties of key aerosol types observed in worldwide locations, J. Atmos. Sci., 59, 590-608, http://doi.org/10.1175/1520-0469(2002)059<0590:VOAAOP>2.0.CO;2, 2002.**

Dubovik, O., Sinyuk, A., Lapyonok, T., Holben, B. N., Mishchenko, M., Yang, P., Eck, T. F., Volten, H., Muñoz, O., and Veihelmann, B.: Application of spheroid models to account for aerosol particle nonsphericity in remote sensing of desert dust, J. Geophys. Res.–Atmos., 111, https://doi.org/10.1029/2005JD006619, 2006.

Eck, T., Holben, B., Reid, J., Dubovik, O., Smirnov, A., O'Neill, N., Slutsker, I., and Kinne, S.: Wavelength dependence of the optical depth of biomass burning, urban, and desert dust aerosols, J. Geophys. Res.–Atmos., 104, 31333-31349, https://doi.org/10.1029/1999JD900923, 1999.

Eck, T., Holben, B., Ward, D., Mukelabai, M., Dubovik, O., Smirnov, A., Schafer, J., Hsu, N., Piketh, S., and Queface, A.: Variability of biomass burning aerosol optical characteristics in southern Africa during the SAFARI 2000 dry season campaign and a comparison of single scattering albedo estimates from radiometric measurements, J. Geophys. Res., 108, https://doi.org/10.1029/2002JD002321, 2003.

Eck, T. F., Holben, B. N., Reid, J. S., Sinyuk, A., Hyer, E. J., O'Neill, N. T., Shaw, G. E., Vande Castle, J. R., Chapin, F. S., Dubovik, O., Smirnov, A., Vermote, E., Schafer, J. S., Giles, D., Slutsker, I., Sorokine, M., and Newcomb, W. W.: Optical properties of boreal region biomass burning aerosols in central Alaska and seasonal variation of aerosol optical depth at an Arctic coastal site, J. Geophys. Res., 114, D11201, https://doi.org/10.1029/2008JD010870, 2009.

Freudenthaler, V., Esselborn, M., Wiegner, M., Heese, B., Tesche, M., Ansmann, A., Müller, D., Althausen, D., Wirth, M., and Fix, A.: Depolarization ratio profiling at several wavelengths in pure Saharan dust during SAMUM 2006, Tellus B, 61, 165-179, https://doi.org/10.1111/j.1600-0889.2008.00396.x, 2009.

Giles, D. M., Holben, B. N., Eck, T. F., Sinyuk, A., Smirnov, A., Slutsker, I., Dickerson, R., Thompson, A., and Schafer, J.: An analysis of AERONET aerosol absorption properties and classifications representative of aerosol source regions, J. Geophys. Res., 117, https://doi.org/10.1029/2012JD018127, 2012.

**Gobbi, G. P., Kaufman, Y. J., Koren, I., and Eck, T. F.: Classification of aerosol properties derived from AERONET direct sun data, Atmos. Chem. Phys., 7, 453-458, https://doi.org/10.5194/acp-7-453-2007, 2007.**

**Groß, S., Tesche, M., Freudenthaler, V., Toledano, C., Wiegner, M., Ansmann, A., Althausen, D., and Seefeldner, M.: Characterization of Saharan dust, marine aerosols and mixtures of biomass-burning aerosols and dust by means of multi-wavelength depolarization and Raman lidar measurements during SAMUM 2, Tellus B, 63, 706-724,doi:10.1111/j.1600-0889.2011.00556.x,2011.**

Guo, J.-P., Zhang, X.-Y., Wu, Y.-R., Zhaxi, Y., Che, H.-Z., La, B., Wang, W., and Li, X.-W.: Spatio-temporal variation trends of satellite-based aerosol optical depth in China during 1980-2008, Atmos. Environ., 45, 6802-6811, https://doi.org/ 10.1016/j.atmosenv.2011.03.068, 2011.

Haywood, J.M. and Ramaswamy, V.: Global sensitivity studies of the direct radiative forcing due to anthropogenic sulfate and black carbon aerosols, J. Geophys. Res.–Atmos., 103, 6043-6058, https://doi.org/10.1029/97JD03426, 1998.

Hess, M., Koepke, P., and Schult, I.: Optical properties of aerosols and clouds: The software package OPAC, Bull. Am. Met. Soc., 79, 831-844, https://doi.org/10.1175/1520-0477(1998)079<0831:OPOAAC>2.0.CO;2, 1998.

Holben, B. N., Eck, T. F., Slutsker, I., Tanré, D., Buis, J., Setzer, A., Vermote, E., Reagan, J., Kaufman, Y. J., and Nakajima, T.: AERONET—A federated instrument network and data archive for aerosol characterization, Rem. Sens. Environ., 66, 1-16, https://doi.org/10.1016/S0034-4257(98)00031-5, 1998.

Jones, T. A. and Christopher, S. A.: MODIS derived fine mode fraction characteristics of marine, dust, and anthropogenic aerosols over the ocean, constrained by GOCART, MOPITT, and TOMS, J. Geophys. Res., 112, https://doi.org/10.1029/2007JD008974, 2007.

Jung, J., Lee, H., Kim, Y. J., Liu, X., Zhang, Y., Hu, M., and Sugimoto, N.: Optical properties of atmospheric aerosols obtained by in situ and remote measurements during 2006 Campaign of Air Quality Research in Beijing (CAREBeijing-2006), J. Geophys. Res., 114, D00G02, https://doi.org/10.1029/2008JD010337, 2009.

Kim, J., Lee, J., Lee, H. C., Higurashi, A., Takemura, T., and Song, C. H.: Consistency of the aerosol type classification from satellite remote sensing during the Atmospheric Brown Cloud–East Asia Regional Experiment campaign, J. Geophys. Res., 112, https://doi.org/10.1029/2006JD008201, 2007.

Lee, J., Kim, J., Song, C., Kim, S., Chun, Y., Sohn, B., and Holben, B.: Characteristics of aerosol types from AERONET sunphotometer measurements, Atmos. Environ., 44, 3110-3117, https://doi.org/10.1016/j.atmosenv.2010.05.035, 2010.

Liu, J., Lin, P., Laskin, A., Laskin, J., Kathmann, S. M., Wise, M., Caylor, R., Imholt, F., Selimovic, V., and Shilling, J. E.: Optical properties and aging of ligh-absorbing secondary organic aerosol, Atmos. Chem. Phys., 16, 12815-12827, https://doi.org/10.5194/acp-16-12815-2016, 2016.

**Mamouri, R. E. and Ansmann, A.: Fine and coarse dust separation with polarization lidar, Atmos. Meas. Tech., 7, 3717-3735, https://doi.org/10.5194/amt-7-3717-2014, 2014.**

**Mamouri, R.-E. and Ansmann, A.: Potential of polarization/Raman lidar to separate fine dust, coarse dust, maritime, and anthropogenic aerosol profiles, Atmos. Meas. Tech., 10, 3403-3427, https://doi.org/10.5194/amt-10-3403-2017, 2017.**

Murayama, T., Müller, D., Wada, K., Shimizu, A., Sekiguchi, M., and Tsukamoto, T.: Characterization of Asian dust and Siberian smoke with multi-wavelength Raman lidar over Tokyo, Japan in spring 2003, Geophys. Res. Lett., 31, https://doi.org/10.1029/2004GL021105, 2004.

Nakata, M., Sano, I., Mukai, S., and Holben, B.N.: Spatiotemporal variations in atmospheric aerosols in East Asia: Identifying local pollutants and transported Asian aerosols in Osaka, Japan using DRAGON, Atmos. Chem. Phys., 16, 14795-14803, https://doi.org/ 10.5194/acp-16-14795-2016, 2016.

Noh, Y., Müller, D., Lee, K., Kim, K., Shimizu, A., Sano, I., and Park, C.B.: Depolarization ratios retrieved by AERONET sun–sky radiometer data and comparison to depolarization ratios measured with lidar, Atmos. Chem. Phys. 17, 6271-6290, https://doi.org/10.5194/acp-17-6271-2017, 2017.

Petzold, A., Rasp, K., Weinzierl, B., Esselborn, M., Hamburger, T., Dörnbrack, A., Kandler, K., Schütz, L., Knippertz, P., Fiebig, M. and Virkkula, A.: Saharan dust absorption and refractive index from aircraft-based observations during SAMUM 2006, Tellus, 61B, 118-130, https://doi.org/10.1111/j.1600-0889.2008.00383.x, 2009.

Petzold, A., Veira, A., Mund, S., Esselborn, M., Kiemle, C., Weinzierl, B., Hamburger, T., Ehret, G., Lieke, K. and Kandler, K.: Mixing of mineral dust with urban pollution aerosol over Dakar (Senegal): Impact on dust physico-chemical and radiative properties, Tellus, 63B, 619-634, https://doi.org/10.1111/j.1600-0889.2011.00547.x, 2011.

Reid, J. S., Hobbs, P. V., Ferek, R. J., Blake, D. R., Martins, J. V., Dunlap, M. R., and Liousse, C.: Physical, chemical and optical properties of regional hazes dominated by smoke in Brazil, J. Geophys. Res., 103, 32059-32080, https://doi.org/10.1029/98JD00458, 1998.

Reid, J. S., Eck, T. F., Christopher, S. A., Koppmann, R., Dubovik, O., Eleuterio, D. P., Holben, B. N., Reid, E. A., and Zhang, J.: A review of biomass burning emissions part II: intensive physical properties of biomass burning particles, Atmos. Chem. Phys., 5, 799-825, https://doi.org/10.5194/acp-5-799-2005, 2005.

Russell, P., Bergstrom, R., Shinozuka, Y., Clarke, A., DeCarlo, P., Jimenez, J., Livingston, J., Redemann, J., Dubovik, O., and Strawa, A.: Absorption Angstrom exponent in AERONET and related data as an indicator of aerosol composition, Atmos. Chem. Phys., 10, 1155-116, https://doi.org/10.5194/acp-10-1155-2010, 2010.

Russell, P. B., Kacenelenbogen, M., Livingston, J. M., Hasekamp, O. P., Burton, S. P., Schuster, G. L., Johnson, M. S., Knobelspiesse, K. D., Redemann, J., and Ramachandran, S.: A multiparameter aerosol classification method and its application to retrievals from spaceborne polarimetry, J. Geophys. Res., 119, 9838-9863, https://doi.org/10.1002/2013JD021411, 2014.

Sano, I., Mukai, S., Nakata, M., and Holben, B. N.: Regional and local variations in atmospheric aerosols using ground-based sun photometry during Distributed Regional Aerosol Gridded Observation Networks (DRAGON) in 2012, Atmos. Chem. Phys., 16, 14795-14803, https://doi.org/10.5194/acp-16-14795-2016, 2016.

Satheesh, S., and Moorthy, K. K.: Radiative effects of natural aerosols: A review, Atmos. Environ., 39, 2089-2110, https://doi.org/10.1016/j.atmosenv.2004.12.029, 2005.

Schuster, G.L., Dubovik, O., Holben, B.N., and Clothiaux, E.E.: Inferring black carbon content and specific absorption from Aerosol Robotic Network (AERONET) aerosol retrievals, J. Geophys. Res.–Atmos., 110, https://doi.org/10.1029/2004JD004548, 2005.

Schuster, G. L., Dubovik, O., and Holben, B. N.: Angstrom exponent and bimodal aerosol size distributions, J. Geophys. Res.–Atmos., 111, https://doi.org/10.1029/2005JD006328, 2006.

Shimizu, A., Sugimoto, N., Matsui, I., Arao, K., Uno, I., Murayama, T., Kagawa, N., Aoki, K., Uchiyama, A., and Yamazaki, A.: Continuous observations of Asian dust and other aerosols by polarization lidars in China and Japan during ACE-Asia, J. Geophys. Res.–Atmos., 109, https://doi.org/10.1029/2002JD003253, 2004.

Shin, S.K., Müller, D., Lee, C., Lee, K.H., Shin, D., Kim, Y.J., and Noh, Y.M.: Vertical variation of optical properties of mixed Asian dust/pollution plumes according to pathway of air mass transport over East Asia, Atmos. Chem. Phys. 15, 6707-6720, https://doi.org/10.5194/acp-15-6707-2015, 2015.

Shin, S.-K., Tesche, M., Kim, K., Kezoudi, M., Tatarov, B., Müller, D., and Noh, Y.: On the spectral depolarisation and lidar ratio of mineral dust provided in the AERONET version 3 inversion product, Atmos. Chem. Phys., 18, 12735-12746, https://doi.org/10.5194/acp-18-12735-2018, 2018.

Shin, S.-K., Tesche, M., Müller, D., and Noh, Y.: Technical note: Absorption aerosol optical depth components from AERONET observations of mixed dust plumes, Atmos. Meas. Tech., 12, 607-618, https://doi.org/10.5194/amt-12-607-2019, 2019.

Stocker, T.F., Qin, D., Plattner, G.-K., Tignor, M., Allen, S.K., Boschung, J., Nauels, A., Xia, Y., Bex, V., Midgley, P.M.: Climate Change 2013: The Physical Science Basis. Contribution of Working Group I to the Fifth Assessment Report of the Intergovernmental Panel on Climate Change, 1535 pp. Cambridge Univ. Press, Cambridge, UK, and New York, 2013.

Sugimoto, N. and Lee, C. H.: Characteristics of dust aerosols inferred from lidar depolarization measurements at two wavelengths, Appl. Opt., 45, 7468-7474, https://doi.org/10.1364/AO.45.007468, 2006.

Sun, Y., Zhuang, G., Wang, Y., Zhao, X., Li, J., Wang, Z., and An, Z.: Chemical composition of dust storms in Beijing and implications for the mixing of mineral aerosol with pollution aerosol on the pathway, J. Geophys. Res., 110, https://doi.org/10.1029/2005JD006054, 2005.

Tesche, M., Ansmann, A., Müller, D., Althausen, D., Engelmann, R., Freudenthaler, V., and Groß, S.: Vertically resolved separation of dust and smoke over Cape Verde using multiwavelength Raman and polarization lidars during Saharan Mineral Dust Experiment 2008, J. Geophys. Res.–Atmos., 114, D13202, 2009.

**Tesche, M., Groß, S., Ansmann, A., Müller, D., Althausen, D., Freudenthaler, V., and Esselborn, M.: Profiling of Saharan dust and biomass-burning smoke with multiwavelength polarization Raman lidar at Cape Verde, Tellus B, 63, 649-676, 2011.**

Twomey, S.: Pollution and the planetary albedo, Atmos. Environ., 8, 1251-1256, https://doi.org/10.1016/0004-6981(74)90004-3, 1974.

Wang, J. and Martin, S. T.: Satellite characterization of urban aerosols: Importance of including hygroscopicity and mixing state in the retrieval algorithms, J. Geophys. Res., 112, https://doi.org/10.1029/2006JD008078, 2007.

**Washenfelder, R. A., Attwood, A. R., Brock, C. A., Guo, H., Xu, L., Weber, R. J., Ng, N. L., Allen, H. M., Ayres, B. R., Baumann, K., Cohen, R. C., Draper, D. C., Duffey, K. C., Edgerton, E., Fry, J. L., Hu, W. W., Jimenez, J. L., Palm, B. B., Romer, P., Stone,**

**E. A., Wooldridge, P. J., and Brown, S. S.: Biomass burning dominates brown carbon absorption in the rural southeastern United States, Geophys. Res. Lett., 42, 653-664, https://doi.org/10.1002/2014GL062444, 2015.**

Xia, X. G., Li, Z. Q., Holben, B., Wang, P. C., Eck, T., Chen, H. B., Cribb, M., and Zhao, Y. X: Aerosol optical properties and radiative effects in the Yangtze Delta region of China, J. Geophys. Res., 112, D22S12, http://doi.org/10.1029/2007JD008859, 2007.

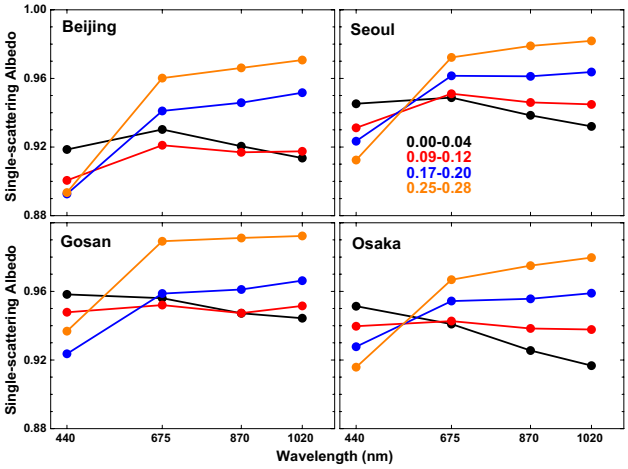


**Figure 1.** The mean spectra of SSA for different ranges of PLDR at the East Asian AERONET sites considered in this study.

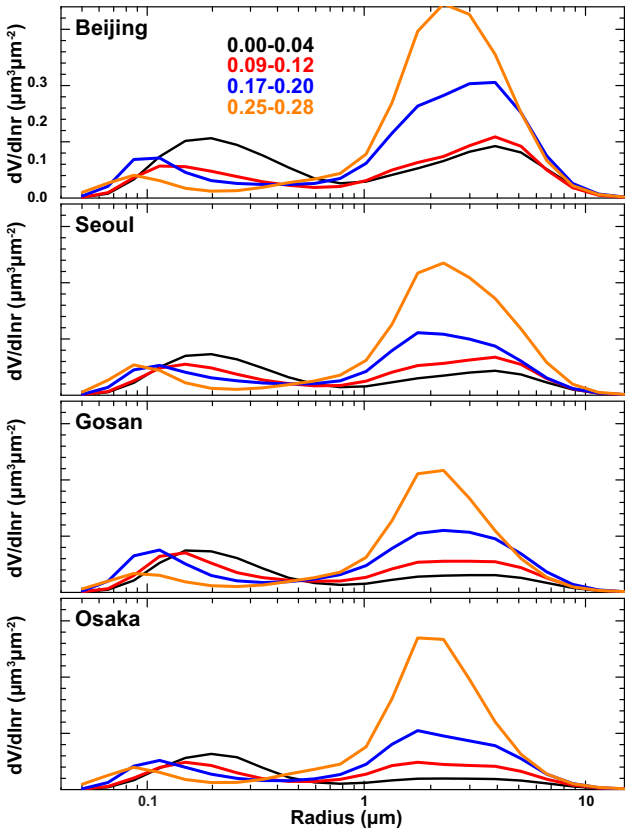


**Figure 2.** The mean volume particle size distributions for different ranges of PLDR for the East Asian AERONET sites considered in this study.

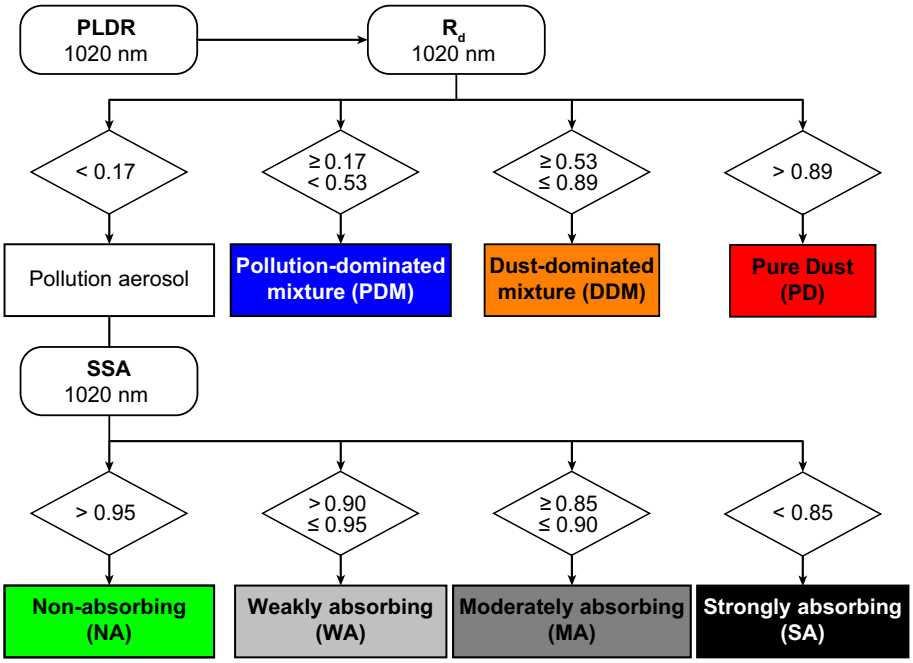


**Figure 3.** Flowchart of the aerosol classification based on the ~~1020-nm PLDR~~ **dust ratio $R_d$ derived using PLDR at 1020 nm** and the 1020-nm SSA that are inferred from the inversion of AERONET observations.

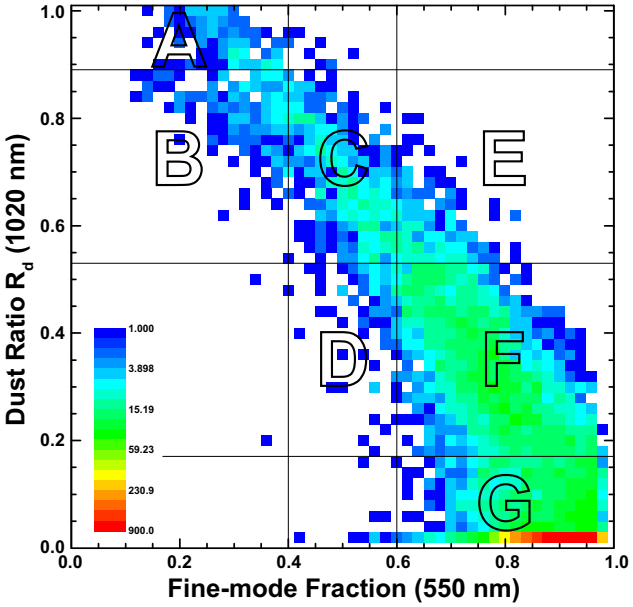


**Figure 4.** Two-dimensional histograms of ~~1020-nm PLDR~~ $R_d$ **derived using PLDR at 1020 nm** and FMF **at 550 nm** for the considered AERONET stations over East Asia. Seven sectors A to G are defined according to the ranges of PLDR and FMF**: pure dust (sector A), dust-dominated mixture (sectors B, C, and E), pollution-dominated mixture (sectors D and E), and pollution (sector G).** The color coding indicates the number of observation data in log scale.

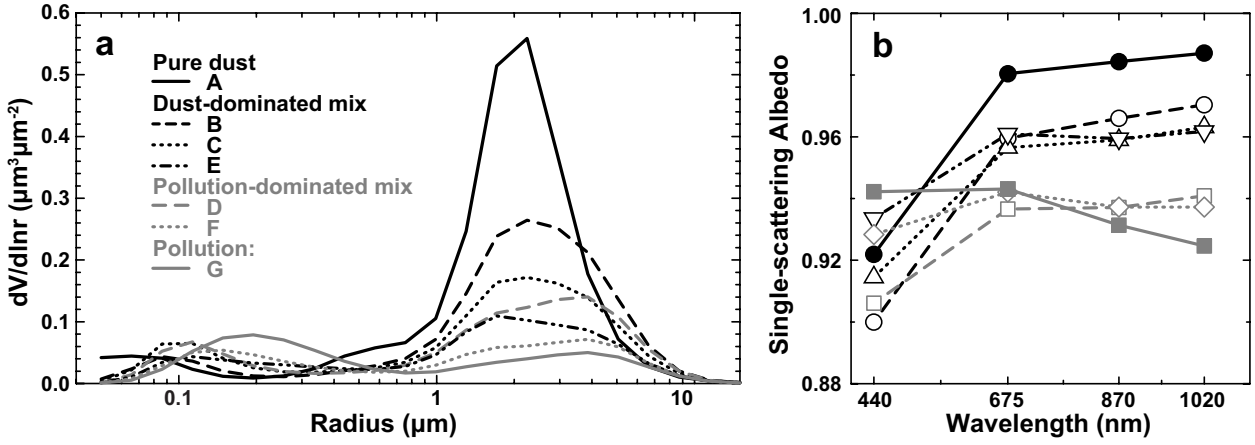


**Figure 5.** Mean volume size distributions (a) and spectral SSA (b) for the aerosol-type sectors identified in Figure 4. **Black lines relate to pure dust (solid lines and circles) and dust-dominated mixtures (dashed lines, open circles and triangles) while gray lines mark pollution (solid lines and squares) and pollution-dominated mixtures (dashed lines, open squares and diamonds).**

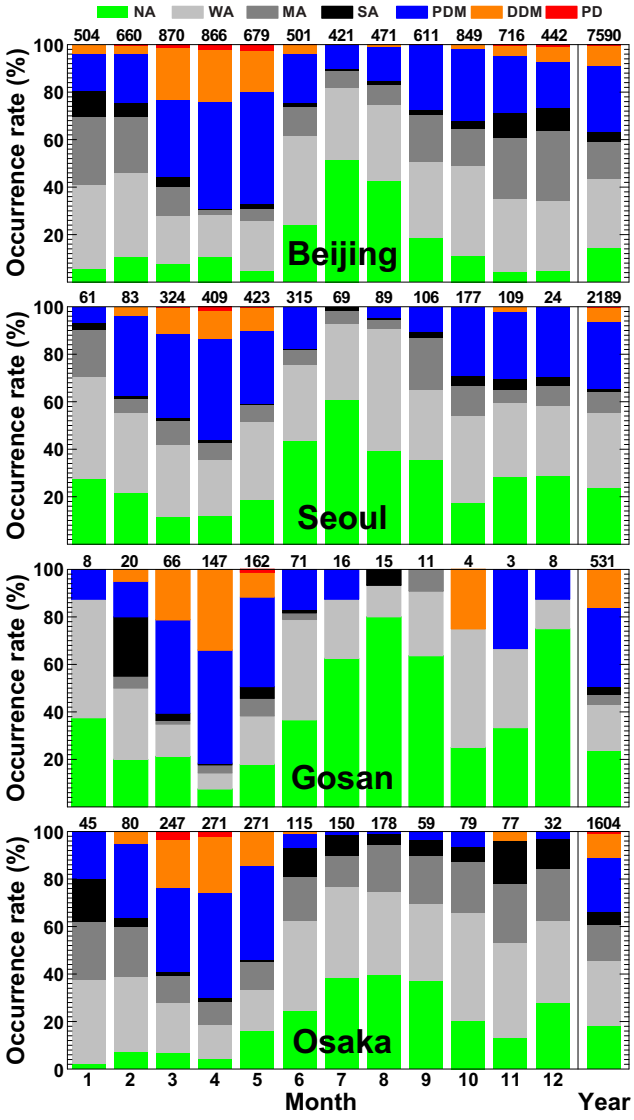


**Figure 6.** ~~O~~ **Monthly and annual o**ccurrence rate of the aerosol types classified according to this study for AERONET observation sites over East Asia. The colour coding refers to the aerosol species introduced in Figure 3. **The numbers above the plots refer to the number of observations for which SSA and PLDR are available in the AERONET data base.**

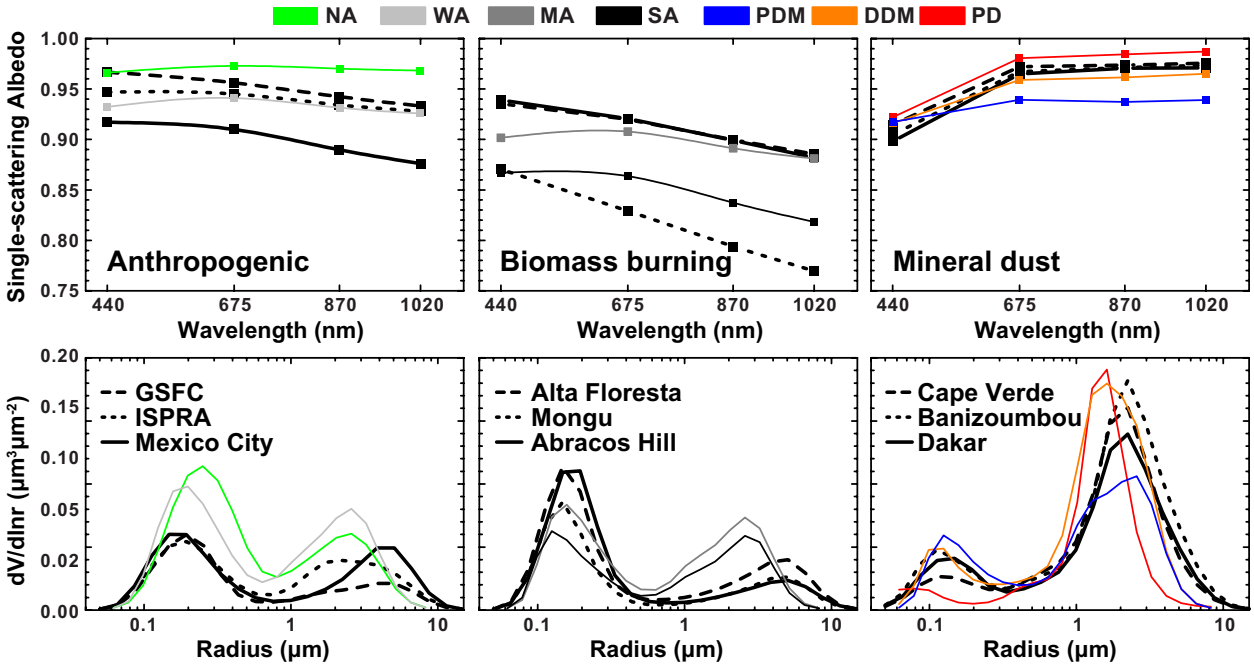


**Figure 7.** Mean spectral SSA (upper row) and mean particle size distributions (lower row) for AERONET sites that are considered as representative for different aerosol types ~~(magenta, yellow and dark green)~~ as well as for the aerosol types defined in this study (see Figure 3 for color coding). Note that the size distribution for pure mineral dust (red line) has been scaled to 50% to fit the plot.

**Table 1.** Geographical/retrieval information for each AERONET site used in this study, along with some references for each aerosol type. **The number of cases refers to observations for which SSA and PLDR are available in the AERONET data base.**

| Site | Latitude [°] | Longitude [°] | Elevation [m] | Years | Cases |
|---|---|---|---|---|---|
| **Greater Beijing** | | | | | |
| Beijing | 39.98 | 116.38 | 92 | 2001-2017 | ~~4480~~ **2713** |
| Xianghe | 39.75 | 116.96 | 36 | 2001-2017 | ~~8289~~ **4827** |
| **Seoul** | | | | | |
| Seoul_SNU | 37.45 | 126.95 | 116 | 2002-2017 | ~~1715~~ **821** |
| Yonsei_University | 37.56 | 126.94 | 97 | 2011-2017 | ~~2784~~ **1367** |
| **Gosan_SNU** | 33.29 | 126.16 | 72 | 2001-2016 | ~~1292~~ **531** |
| **Osaka** | | | | | |
| Osaka | 34.65 | 135.59 | 50 | 2000-2016 | ~~2392~~ **700** |
| Shirahama | 33.69 | 135.36 | 10 | 2000-2016 | ~~4080~~ **904** |
| **Dust** | | | | | |
| Banizoumbou | 13.55 | 2.67 | 274 | 1995-2018 | 4217 |
| Capo_Verde | 16.73 | -22.94 | 60 | 1994-2018 | 1612 |
| Dakar | 14.39 | -16.96 | 21 | 1996-2018 | 3676 |
| **Biomass burning** | | | | | |
| Abrascos Hill | -10.76 | -62.36 | 259 | 1999-2015 | 392 |
| Mongu | -15.25 | 23.15 | 1047 | 1995-2010 | 1276 |
| Alta Floresta | -9.87 | -56.10 | 277 | 1993-2018 | 817 |
| **Anthropogenic** | | | | | |
| GSFC | 38.99 | -76.84 | 87 | 1993-2018 | 1237 |
| Ispra | 45.80 | 8.63 | 235 | 1997-2018 | 1114 |
| Mexico City | 19.33 | -99.18 | 2268 | 1999-2017 | 692 |

**Table 2.** Average values of AERONET-derived aerosol parameters for the sectors identified in Figure 5: FMF, AOD-related Ångström exponent for the wavelength pair 440 and 870 nm (AE), PLDR at 1020 nm, SSA at 1020 nm, total volume concentration (VolC), effective radius (Reff), and the volume median radius (VMR). For comparison, *Lee et al.* (2010) classifies categories A and B as dust, categories C and D as mixed, and categories E, F, and G as pollution.

| | **A** pure dust (PD) | **B** dust dominated (DDM) | **C** dust dominated (DDM) | **D** pollutant dominated (PDM) | **E** dust dominated (DDM) | **F** pollutant dominated (PDM) | **G** pollution |
|---|---|---|---|---|---|---|---|
| N | 90 | 355 | 520 | 207 | 512 | 3488 | 6691 |
| FMF | 0.31±0.18 | 0.41±0.17 | 0.59±0.13 | 0.62±0.09 | 0.71±0.09 | 0.80±0.08 | 0.90±0.05 |
| ~~AE~~ | ~~0.50±0.45~~ | ~~0.41±0.22~~ | ~~0.46±0.22~~ | ~~0.52±0.28~~ | ~~0.56±0.33~~ | ~~0.60±0.50~~ | ~~0.65±0.61~~ |
| **AE** | **0.17±0.08** | **0.38±0.15** | **0.70±0.14** | **0.83±0.11** | **0.88±0.14** | **1.17±0.15** | **1.36±0.19** |
| PLDR | 0.28±0.04 | 0.22±0.03 | 0.17±0.03 | 0.13±0.02 | 0.16±0.02 | 0.09±0.02 | 0.02±0.01 |
| ~~SSA~~ | ~~0.90±0.26~~ | ~~0.88±0.25~~ | ~~0.84±0.31~~ | ~~0.87±0.22~~ | ~~0.88±0.26~~ | ~~0.87±0.21~~ | ~~0.85±0.25~~ |
| **SSA** | **0.99±0.01** | **0.97±0.01** | **0.96±0.01** | **0.94±0.01** | **0.96±0.01** | **0.94±0.01** | **0.92±0.01** |
| VolC | 0.52±0.31 | 0.44±0.27 | 0.38±0.18 | 0.40±0.15 | 0.38±0.21 | 0.40±0.23 | 0.50±0.30 |
| Reff | 0.73±0.36 | 0.59±0.33 | 0.40±0.20 | 0.43±0.19 | 0.37±0.15 | 0.30±0.12 | 0.28±0.11 |

**Table 3.** Occurrence rate (in percent ~~and absolute numbers~~) of the aerosol types identified with our method at the AERONET sites given in the lower half of Table 1.

| | **cases** | **PD** | **DDM** | **PDM** | **NA** | **WA** | **MA** | **SA** |
|---|---|---|---|---|---|---|---|---|
| **Anthropogenic** | | | | | | | | |
| GSFC | 1237 | ~~0 (0%)~~ | ~~0 (0 %)~~ | ~~15 (1 %)~~ | ~~421 (34 %)~~ | ~~587 (47 %)~~ | ~~192 (16 %)~~ | ~~22 (2 %)~~ |
| Ispra | 1114 | ~~0 (0 %)~~ | ~~0 (0 %)~~ | ~~72 (6 %)~~ | ~~353 (32 %)~~ | ~~414 (37 %)~~ | ~~212 (19 %)~~ | ~~58 (5 %)~~ |
| Mexico City | 692 | ~~0 (0 %)~~ | ~~0 (0 %)~~ | ~~12 (2 %)~~ | ~~72 (10 %)~~ | ~~166 (24 %)~~ | ~~238 (34 %)~~ | ~~204 (29 %)~~ |
| **Biomass burning** | | | | | | | | |
| Alta Floresta | 817 | ~~0 (0 %)~~ | ~~0 (0 %)~~ | ~~6 (1 %)~~ | ~~31 (4 %)~~ | ~~275 (34 %)~~ | ~~341 (42 %)~~ | ~~164 (20 %)~~ |
| Mongu | 1276 | ~~0 (0 %)~~ | ~~0 (0%)~~ | ~~0 (0%)~~ | ~~4 (0%)~~ | ~~3 (0%)~~ | ~~50 (4%)~~ | ~~1219 (96%)~~ |
| Abracos Hill | 392 | ~~0 (0 %)~~ | ~~0 (0%)~~ | ~~0 (0%)~~ | ~~15 (4%)~~ | ~~135 (34%)~~ | ~~160 (41%)~~ | ~~82 (21%)~~ |
| **Saharan Dust** | | | | | | | | |
| Capo Verde | 1612 | ~~1311 (81 %)~~ | ~~260 (16 %)~~ | ~~29 (2 %)~~ | ~~1 (0 %)~~ | ~~0 (0 %)~~ | ~~3 (0 %)~~ | ~~7 (0 %)~~ |
| Banizoumbou | 4217 | ~~2749 (65 %)~~ | ~~1268 (30 %)~~ | ~~185 (4 %)~~ | ~~0 (0 %)~~ | ~~1 (0 %)~~ | ~~5 (0 %)~~ | ~~4 (0 %)~~ |
| Dakar | 3676 | ~~2204 (64 %)~~ | ~~1214 (35 %)~~ | ~~0 (0 %)~~ | ~~4 (0 %)~~ | ~~6 (0 %)~~ | ~~1 (0 %)~~ | ~~11 (0 %)~~ |